International Journal of Biological Macromolecules

Assessment of Catalytic, Antimicrobial and Molecular Docking Analysis of Starch-Grafted Polyacrylic Acid Doped BaO Nanoparticles

--Manuscript Draft--

Manuscript Number:	IJBIOMAC-D-22-10751R1
Article Type:	Research Paper
Section/Category:	Carbohydrates, Natural Polyacids and Lignins
Keywords:	starch; BaO; catalysis
Corresponding Author:	Muhammad Ikram Government College University Lahore Department of Physics Lahore, Pakistan PAKISTAN
First Author:	Muhammad Ikram
Order of Authors:	Muhammad Ikram
	Ali Haider
	Muhammad Imran
	Junaid Haider
	Sadia Naz
	Anwar Ul-Hamid
	Anum Shahzadi
	Kinza Ghazanfar
	Walid Nabgan
	Sawaira Moeen
	Salamat Ali
Abstract:	The removal of cationic dyes from water has received a great attention of researchers considering their influence on environment and ecosystem. In current work, starch-grafted-poly acrylic acid (St-g-PAA) doped BaO nanoparticles have been synthesized by co-precipitation approach. The aim of this research was to reduce the harmful methylene blue dye and evaluate the antibacterial activity of St-g-PAA doped BaO. XRD spectra exhibited the tetragonal structure of BaO and no variations occurred upon doping. The optical properties of St-g-PAA doped BaO have been evaluated by UV–Vis spectrophotometer. The existence of a dopant in the product was verified using EDS spectroscopy. TEM revealed the formation of cubic-shaped NPs of BaO and upon the addition of St-g-PAA, a few nanorod-like structures. The higher concentration of St-g-PAA doped BaO exhibit a remarkable reduction of methylene blue in a basic environment. Furthermore, St-g-PAA doped BaO revealed higher antimicrobial efficacy against Staphylococcus aureus in comparison to Escherichia coli. In silico studies were conducted against enoyl-[acylcarrier-protein] reductase (FabI) and beta-lactamase enzyme to evaluate the potential of both St-g-PAA and St-g-PAA doped BaO nanocomposites as their inhibitors and to rationalize their possible mode of action.
Suggested Reviewers:	Dayong Wu dayongwu@mail.ipc.ac.cn
	Alberto Naldoni alberto.naldoni@upol.cz
	M Tahir m.tahir@utm.my
Opposed Reviewers:	
Response to Reviewers:	Reviewer #1: Comments - further recommendations

	I hope these comments are helpful. General Comments This study aimed to synthesize starch-grafted-poly acrylic acid (St-g-PAA) doped BaO nanoparticles by co-precipitation for catalytic and bactericidal activities. The article may be acceptable for publication after the authors made some revisions. Specific Comments 1. Graphical Abstract: - The authors should provide a graphical abstract to support the manuscript. Ans: Graphical abstract has been added in manuscript. 2. Abstract: - The author should re-arrange and re-write the abstract in the following order (Problem of research, aim of study, remarkable methodology, remarkable results, and significance of study). Ans: It has been revised according to suggestion. 3. Introduction: - The authors should provide this study's aim and significance by the end of this section in a clear format (not the conclusion) Ans: It was incorporated in introduction part. 4. Materials and Methods: - The authors should provide the relevant references to some sub-sections. Ans: The relevant references added in the sub section 5. Conclusions: - The authors should move the last part of the introduction section to the conclusions part and also support it with recommendations and future perspectives. Ans: We have modified the conclusion section accordingly. Editorial Comments 1. The authors should apply the guidelines for authors in general on the whole manuscript (e.g., several editing corrections, References formatting style and order within the text, and also the formatting of the list of references, etc.). Ans: Revised as per guidelines.

Declaration of interests/Conflict of Interest

☒ The authors declare that they have no known competing financial interests or personal relationships that could have appeared to influence the work reported in this paper.
This manuscript has no conflict of interest

Dr. Muhammad Ikram
Assistant Professor Physics
GC University Lahore

Editor-in-Chief
International Journal of Biological Macromolecules
Dear Editor,

We are submitting our manuscript entitled “Assessment of Catalytic, Antimicrobial and Molecular Docking Analysis of Starch-Grafted Polyacrylic Acid Doped BaO Nanoparticles” by authors for review and, if acceptable, for publication in International Journal of Biological Macromolecules.

This paper contains evidence and discussion of In this study, starch-grafted-poly acrylic acid (St-g-PAA) doped BaO nanoparticles were produced for catalytic and bactericidal activity. The structural, chemical, optical, and morphological properties of materials were analysed. XRD spectrum showed BaO's tetragonal structure without doping. The UV–Vis spectroscopy of St-g-PAA doped BaO samples showed a redshift in electronic spectra and a reduction in band gap energy. EDS spectroscopy revealed the elemental composition of a doped product. TEM showed cubic-shaped BaO NPs and nanorod-like structures that overlapped NPs. St-g-PAA doped BaO reduces methylene blue in base. Also, antibacterial effectiveness was tested against Escherichia coli and Staphylococcus aureus. In silico experiments were done against enoyl-[acylcarrier-protein] reductase (FabI) and beta-lactamase enzyme to assess St-g-PAA and St-g-PAA doped BaO nanocomposites as inhibitors and to justify their likely method of action. As such, we believe this manuscript would be of interest to those working in the field and is suitable for International Journal of Biological Macromolecules.

The manuscript, or its contents in some other form, has not been published previously by any of the authors and/or is not under consideration for publication in another journal at the time of submission. In the hope you will find this article worthy of publication in your prestigious journal and thanking you in anticipation,

Thank you,
Sincerely,
Dr. M. Ikram

Reviewer #1: Comments - further recommendations

I hope these comments are helpful.

General Comments

This study aimed to synthesize starch-grafted-poly acrylic acid (St-g-PAA) doped BaO nanoparticles by co-precipitation for catalytic and bactericidal activities. The article may be acceptable for publication after the authors made some revisions.

¬ Specific Comments

1. Graphical Abstract: - The authors should provide a graphical abstract to support the manuscript.

Ans: Graphical abstract has been added in manuscript.

2. Abstract: - The author should re-arrange and re-write the abstract in the following order (Problem of research, aim of study, remarkable methodology, remarkable results, and significance of study).

Ans: It has been revised according to suggestion.

3. Introduction: - The authors should provide this study's aim and significance by the end of this section in a clear format (not the conclusion)

Ans: It was incorporated in introduction part.

4. Materials and Methods: - The authors should provide the relevant references to some sub-sections.

Ans: The relevant references added in the sub section

5. Conclusions: - The authors should move the last part of the introduction section to the conclusions part and also support it with recommendations and future perspectives.

Ans: We have modified the conclusion section accordingly.

¬ Editorial Comments

1. The authors should apply the guidelines for authors in general on the whole manuscript (e.g., several editing corrections, References formatting style and order within the text, and also the formatting of the list of references, etc.).

Ans: Revised as per guidelines.

Author Statement

Muhammad Ikram, Conceptualization, Supervision

Ali Haider, Methodology and Writing

Muhammad Imran, Review and Editing

Junaid Haider, Software and Formal Analysis

Sadia Naz, Data Curation and writing

Anwar Ul-Hamid, Resources and Review and Editing

Anum Shahzadi, Software and Formal Analysis

Kinza Ghazanfar, Writing

Walid Nabgan, Review and Editing

Sawaira Moeen, Writing

Salamat Ali, Supervision

Graphical Abstract

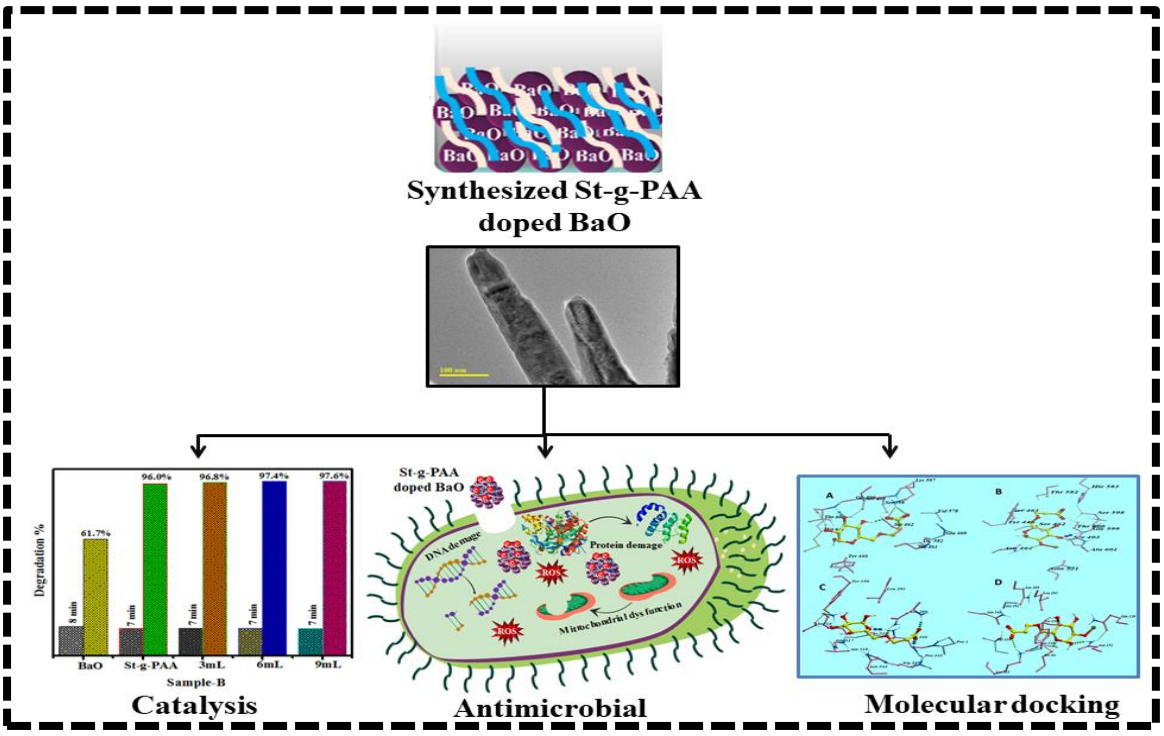

Synthesized St-g-PAA doped BaO for catalytic and bactericidal behavior with molecular docking analysis

Assessment of Catalytic, Antimicrobial and Molecular Docking Analysis of Starch-Grafted Polyacrylic Acid Doped BaO Nanoparticles

Muhammad Ikram[a*], Ali Haider[b], Muhammad Imran[c], Junaid Haider[d], Sadia Naz[d], Anwar Ul-Hamid[e], Anum Shahzadi[f], Kinza Ghazanfar[g], Walid Nabgan[h*], Sawaira Moeen[a], Salamat Ali[g]

[a]Solar Cell Applications Research Lab, Department of Physics, Government College University Lahore, 54000, Pakistan

[b]Department of Clinical Sciences, Faculty of Veterinary and Animal Sciences, Muhammad Nawaz Shareef University of Agriculture, Multan, 66000, Pakistan

[c]Department of Chemistry, Government College University Faisalabad, Pakpattan Road, Sahiwal, Punjab, 57000, Pakistan

[d]Tianjin Institute of Industrial Biotechnology, Chinese Academy of Sciences, Tianjin 300308, China.

[e]Core Research Facilities, King Fahd University of Petroleum & Minerals, Dhahran, 31261, Saudi Arabia

[f]Faculty of Pharmacy, The University of Lahore, Lahore, 54000, Pakistan

[g]Department of Physics, Riphah Institute of Computing and Applied Sciences (RICAS), Riphah International University, 14 Ali Road, Lahore, Pakistan

[h]Departament d'Enginyeria Química, Universitat Rovira i Virgili, Av Països Catalans 26, 43007 Tarragona, Spain

*Corresponding author email: [a]dr.muhammadikram@gcu.edu.pk, [h]wnabgan@gmail.com

ABSTRACT

The removal of cationic dyes from water has received a great attention of researchers considering their influence on environment and ecosystem. In current work, starch-grafted-poly acrylic acid (St-g-PAA) doped BaO nanoparticles have been synthesized by co-precipitation approach. The aim of this research was to reduce the harmful methylene blue dye and evaluate the antibacterial activity of St-g-PAA doped BaO. XRD spectra exhibited the tetragonal structure of BaO and no variations occurred upon doping. The optical properties of St-g-PAA doped BaO have been evaluated by UV–Vis spectrophotometer. The existence of a dopant in the product was verified using EDS spectroscopy. TEM revealed the formation of cubic-shaped NPs of BaO and upon the addition of St-g-PAA, a few nanorod-like structures. The higher concentration of St-g-PAA doped BaO exhibit a remarkable reduction of methylene blue in a basic environment. Furthermore, St-g-PAA doped BaO revealed higher antimicrobial efficacy against *Staphylococcus aureus* in comparison to *Escherichia coli*. *In silico* studies were conducted against enoyl-[acylcarrier-protein] reductase (FabI) and beta-lactamase enzyme to evaluate the potential of both St-g-PAA and St-g-PAA doped BaO nanocomposites as their inhibitors and to rationalize their possible mode of action.

Keywords: Starch; BaO; catalysis

1. INTRODUCTION

Water is a basic component for the existence of the living organism. Only 0.03% of water on earth's surface is fresh, and it is found in water reservoirs like freshwater lakes and rivers [1]. Rapid urbanization and industrialization have a direct negative influence on the environment and human lives. Numerous industries regularly generate harmful dyes as waste products, including the leather, textiles, paper, cosmetics, and food industries [2–5]. Heavy metals and other organic

and inorganic contaminants, including phenols, dyes, polyaromatic hydrocarbons, pesticides, and mineral acids, are found in industrial wastewater along with sulphate, inorganic salts, and trace elements [2,6,7]. Pesticides used on farms, radioactive and industrial waste, marine dumping, and a deteriorating sewage system are all contributing factors that have made contamination a significant issue worldwide. The environment and human life are negatively and destructively affected by water contamination [2,8–10]. Methylene blue (MB), a cationic dye that is widely used in a variety of industries, including the production of paper, food processing, the fashion industry, and printing, has been identified as a concerning cause of water pollution.

Additionally, Gram-positive (G +ve) and Gram-negative (G-ve) microbes are examples of water-borne pathogens that can infect humans. The current state of affairs makes it a global challenge to ensure clean water, making the removal of dyes from aqueous media an essential element [4,11,12]. The impurities from industrial water have been removed using membrane filtering, reverse osmosis, photocatalysis, electrolysis, ion exchange, filtration process, , and microbial control [13].

One of these methods that play an important role in effectively reducing hazardous contaminants is catalysis. It is cost-effective, energy-efficient, and environmentally safe [4]. Transition metal oxides (TMO) are the semiconductor materials that finds numerous uses in photocatalytic degradation, and catalysis [14]. Due to their extensive study and varied applications, TMO, such as CuO, iron oxide, BaO, SnO_2, and ZnO are viewed as one of the wealthiest nanomaterial families [15]. Due to its wide band gap (4.4 eV) and hygroscopic properties, as well as its extensive applications in the fields of self-cleaning, pharmaceutical industry, electrical energy generation, and sensors, researchers have found great interest in BaO NPs [16]. Various

approaches have been used to synthesize BaO NPs with different sizes and shapes, as sol-gel, co-precipitation, and hydrothermal and thermal decomposition [17].

Among these techniques, the co-precipitation technique has gained attention in the industry due to its simple and direct synthesis, and energy-efficient and affordable approach for good yields and mass production [18]. Due to their low cost and ease of processing, polymers such as polyacrylic acid, and polyvinyl pyrrolidone (PVP), among others, have been extensively utilized as dopants [19]. Because of the existence of the carboxyl group, PAA demonstrated a significant capability for the reduction of heavy metal ions and MB from polluted water, along with high antibacterial efficacy. Additionally, PAA based-Nano composites (PAA-TiO_2) have been widely used in optical devices, solar cells, wastewater treatment, and protective covering [20–22]. A class of natural polymers called polysaccharides, including starch, chitosan, inulin, and alginate, are abundant in functional groups like hydroxyl, amino groups, and carboxyl, have favorable chelation and dispersion effects [23]. In recent biopolymer developments, natural polysaccharides have been emphasized as therapeutic agents. Starch and chitosan can be used as adsorbent materials in wastewater treatment because they are biodegradable and don't contain toxins [24]. Based on the above, we believe that using St-g-PAA-doped BaO nanoparticles (NPs) as a catalyst to remove wastewater are a viable option. Additionally, antibacterial activity of pristine and doped BaO NPs was also evaluated. *In silico*, docking studies were also performed to evaluate possible modes of action for both St-g-PAA and St-g-PAA doped BaO nanocomposites against given enzyme targets, i.e., enoyl-[acylcarrier-protein] reductase (FabI) and beta-lactamase from both *E. coli* and *S. aureus*. The synthesis of St-g-PAA-doped BaO oxide NPS was accomplished by the use of co-precipitation, which is a method that is simple, easy to reproduce, and inexpensive.

2. **EXPERIMENTAL SECTION**

2.1 Material Section

($BaCl_2$ $2H_2O$, 99%), sodium hydroxide (NaOH, 98.5%), starch ($C_6H_{10}O_5$), poly acrylic acid $(C_3H_4O_2)n$, and potassium sulphate (K_2SO_4).

2.2 Synthesis of Starch grafted polyacrylic acid

To synthesize starch-grafted polyacrylic acid, the desired amount of starch and acrylic acid (1:3) was added in 200 mL distilled water under vigorous stirring as elaborated in Fig. 1(a). 2 mg of potassium persulphate has been incorporated into the solution and stirred at 70 °C for 5 hours [25].

2.3 Synthesis of St-g-PAA doped BaO

To synthesize BaO NPs, $BaCl_2$. $2H_2O$ (0.5 M) was prepared under robust stirring at 90 °C for 30 minutes. Precipitating agent (NaOH) was integrated drop wise in above solution to sustain pH~ 12. Moreover, the stirred solution has been centrifuged at 7000 rpm and then dried at 160 °C overnight. The acquired BaO was crushed into fine powder. Similarly, different concentrations of St-g-PAA doped BaO were prepared by the cop-precipitation approach, as discussed earlier and demonstrated in Fig. 1(b) [26].

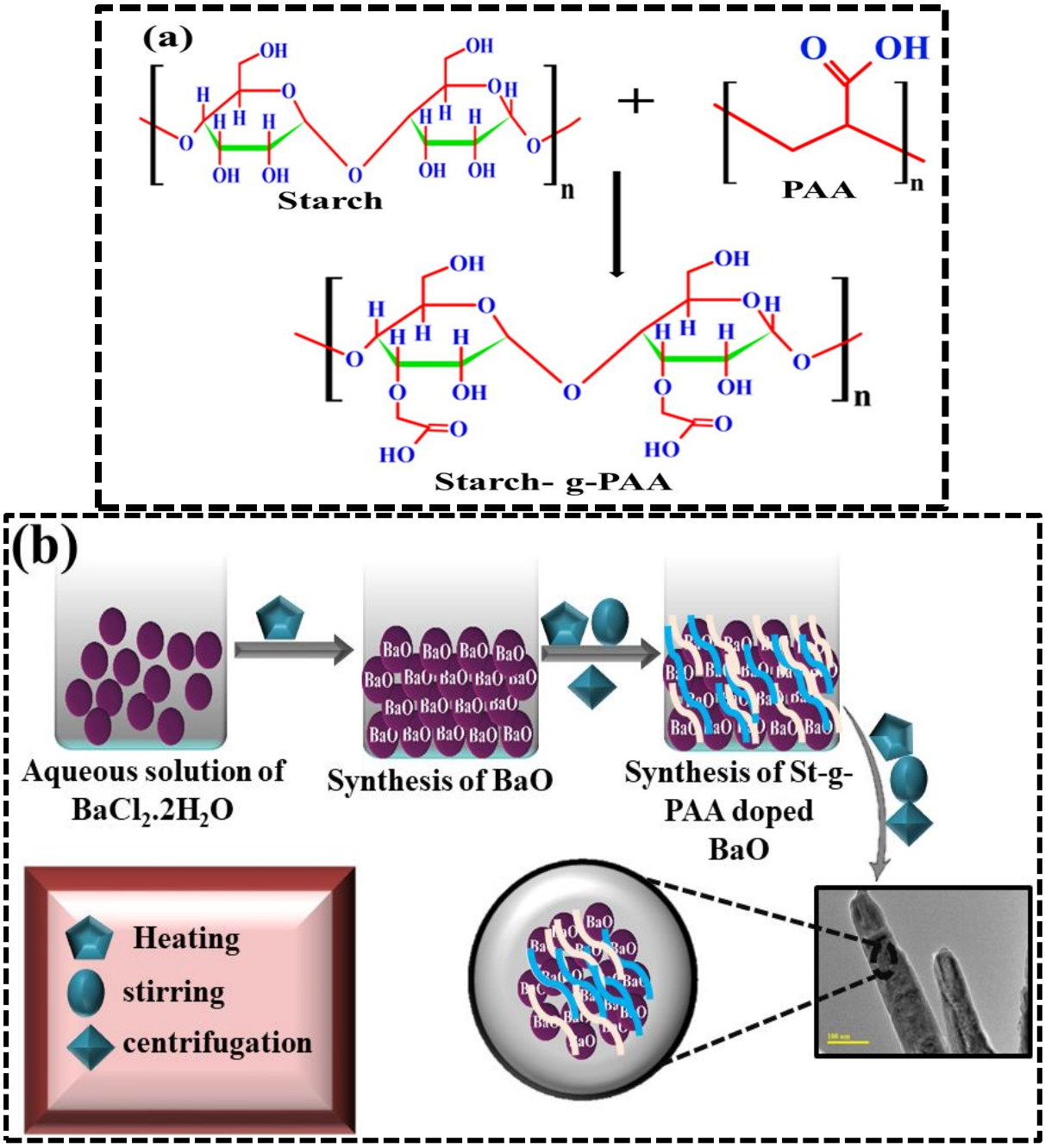

Fig.1 (a) Mechanism of St-g-PAA and (b) Synthesis of St-g-PAA doped BaO NPs

2.4 Catalytic Activity

The catalytic activity (CA) of BaO, St-g-PAA, and incorporated BaO NPs were examined by MB reduction in the existence of $NaBH_4$. The de-colorization of dye was observed at constant intervals by mixing the 400 µL $NaBH_4$ solution with 3mL MB solution. After that, 400 µL of

synthesized samples were incorporated and stirred at ambient temperature to above solution. UV-Vis spectrophotometer was operated to check the MB reduction efficacy in the wavelength range from 200-800 nm.

2.5 Catalysis mechanism

During CA, shifting an electron from $NaBH_4$ (reducing agent) to MB (oxidizing agent) stimulates the redox reaction, causing the dye breakdown as illustrated in Fig. 2. However, the de-colorization of MB in the occurrence of $NaBH_4$ was time-consuming. The incorporation of pristine and doped BaO in above reaction acts as an electron relay that shifts the electron from BH_4^- to MB. The shape, surface area, and crystallinity of prepared NPs influence the CA.

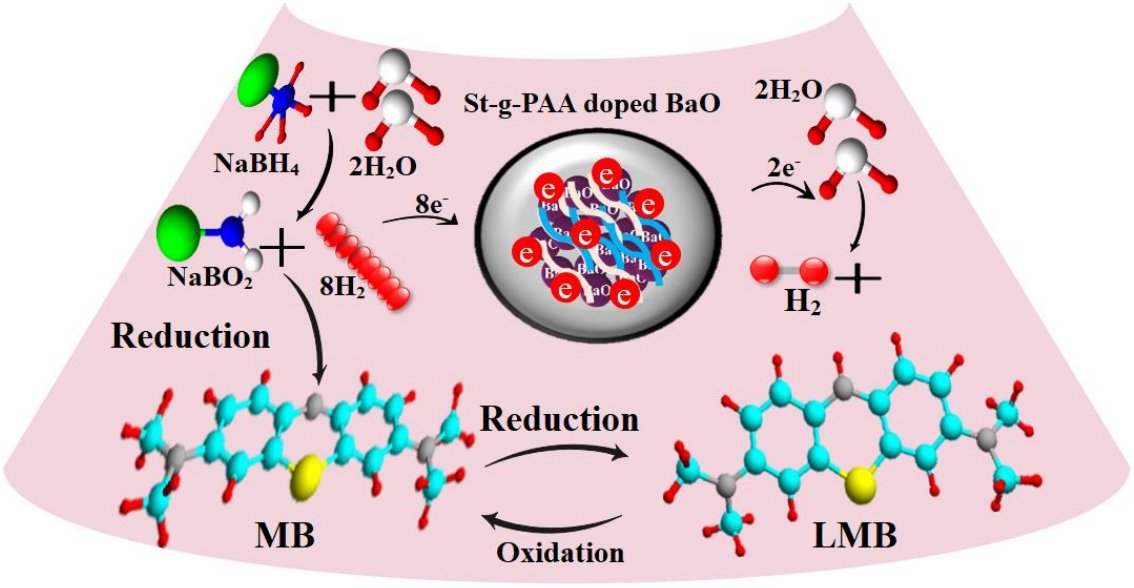

Fig. 2 Catalysis of St-g-PAA doped BaO NPs

2.6 Isolation of *S. aureus* and *E. coli*

Bovine mastitis fluids were acquired from different hospitals and cultivated at 5% blood agar and incubated for 1 day. The obtained colonies were strained on Mannitol salt agar (MSA) and

MacConkey agar (MA) to identify G ±ve microbes, respectively. Biochemical (coagulase and catalase) and gram staining techniques were utilized to isolate distinct colonies.

2.7 Antimicrobial Activity

The bactericidal efficacy of pure and doped BaO was assessed using agar well diffusion methods to test its effectiveness against isolated G +ve and G –ve microbes. After swabbing the MSA and MA deposited petri dish with isolated G +ve and G –ve cultures (1.5 x 108 CFU mL^{-1}), wells with a diameter of 6 mm were created in the MSA and MA petri dish using a sterile cork borer. Each sample was fed into wells at 500 µg/50 µL as the lowest and 1000 µg/50 µL as the highest concentration, compared to standard ciprofloxacin (5 µg/50 µL) and negative control 50 µL DI water without targeted sample. To determine whether or not NPs had an antibacterial effect, prepared plates were left in an incubator at 37 degrees Celsius for 24–48 hours. After incubation for 48 hours, an inhibition area was determined using a Vernier caliper (in millimeters), and the correlation between that area and doping levels was investigated

2.8 Molecular docking studies

Molecular docking predictions were conducted against enoyl-[acylcarrier-protein] reductase (FabI) and beta-lactamase enzyme as both these are essential for bacterial growth [27]. The 3D structural coordinates of selected enzyme targets were achieved from the protein data repository (https://www.rcsb.org/), with PDB ID as 4CUZ for $FabI_{S.\ aureus}$ [28], 4D46 for $FabI_{E.coli}$ [29], 1MWU for beta $lactamase_{S.\ aureus}$ [30], and 4KZ6 for beta $lactamase_{E.\ coli}$ [31]. ICM Molsoft was employed to conduct docking studies [32]. The protein structures were prepared using a multiple-step process, i.e., 1. Removal of H_2O molecules as well as native ligands, 2. Addition of polar H-atoms and gastegier charges, 3. Optimization of protein structure using energy minimization tool of Molsoft. Binding site was identified by specifying 10 Å area around native

ligand. Top ten docked conformation were produced in each case to get the best-docked pose of a stable complex.

Ligands structure were prepared using ligedit tool of Molsoft by modifying starch monomer structure retrieved from PubChem and stable conformation was generated for both nanocomposites in current study. 3D visualizers of Molsoft and PyMOL were used for analysis and graphical representations.

3 RESULTS AND DISCUSSION

The crystallinity of pure, dopant, and St-g-PAA incorporated BaO NPs were investigated through XRD in the 2θ range of 20°–75° (Fig. 3a). The characteristics peaks at 26.9° (101), 33.10° (110), 41° (111), 51°(201), and 60° (220) attributed to the tetragonal structure of BaO NPs along space group P4/nmm (JCPDS Card No 26-0178) [33]. Furthermore, the peak of St was observed at 25.5°. Since the PAA was incorporated into St crystalline structure, the mixtures became amorphous [34]. An additional peak was sited at 39° attributed to potassium persulphate, which was utilized in the preparation of St-g-PAA [35]. Using Scherrer's formula, the average crystallite size of the BaO and doped BaO was observed from 14.2 to 9.09 nm. The broadness of peaks was increased upon doping of St-g-PAA assigned to a decrease in the crystallinity of the NPs due to the amorphous behavior of dopant [36].

To investigate the functional group presence in BaO, dopant, and doped NPs, FTIR spectra have been utilized in range of 4000 to 500 cm^{-1}, as indicated in Fig. 3(b). The transmission band at 692 cm^{-1} represents the Ba–O bond and band at 1455 cm^{-1} might be attributed to the production of barium carbonate as a result of atmospheric CO_2 absorption by BaO [16]. The bands at 1630 and 3313 cm^{-1} indicate the H_2O symmetric vibration and O-H stretching vibration,

correspondingly. The symmetric and asymmetric COO^- stretching of acrylic acid is represented by dopant bands at 1400 and 600 cm^{-1}, respectively [37]. Additionally, SAED analysis shows bright rings related to planes (110), (222), and (202) of BaO and doped BaO (Fig. 3c-f).

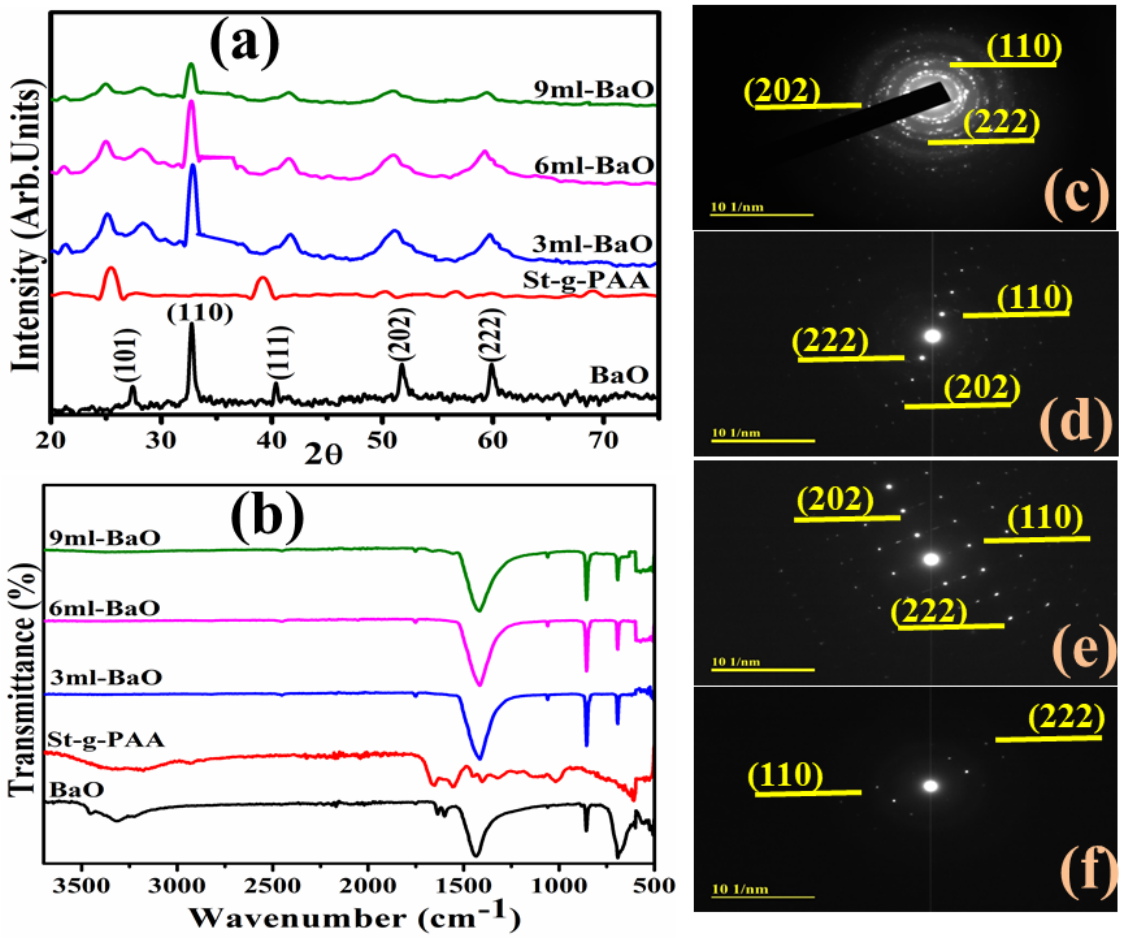

Fig. 3 (a) XRD pattern (b) FTIR spectra of BaO, dopant, and doped NPs, and (c-f) SAED patterns of pure and St-g-PAA (3,6, &9mL) doped BaO NPs respectively.

Electronic spectroscopy was employed to determine the electronic structure of synthesized NPs (Fig .4a). The light absorption of undoped BaO was seen around ~ 310 nm is attributed to the shifting of an electron from 2p of VB of O to Ba of CB correspondingly [26]. Upon doping of St-g-PAA, a red shift was observed, pointing to morphological effects with multiple active sites or possibly a quantum confinement process [38]. The direct bandgap energy of BaO, dopant,

and incorporated BaO were found to be 4.00-3.79 eV by Tauc's equation as illustrated in Fig .4(b). The low orientation rearrangement and less crystallinity of NPs may have contributed to the Eg of the St-g-PAA doped BaO decreasing as the crystallite size reduced [36].

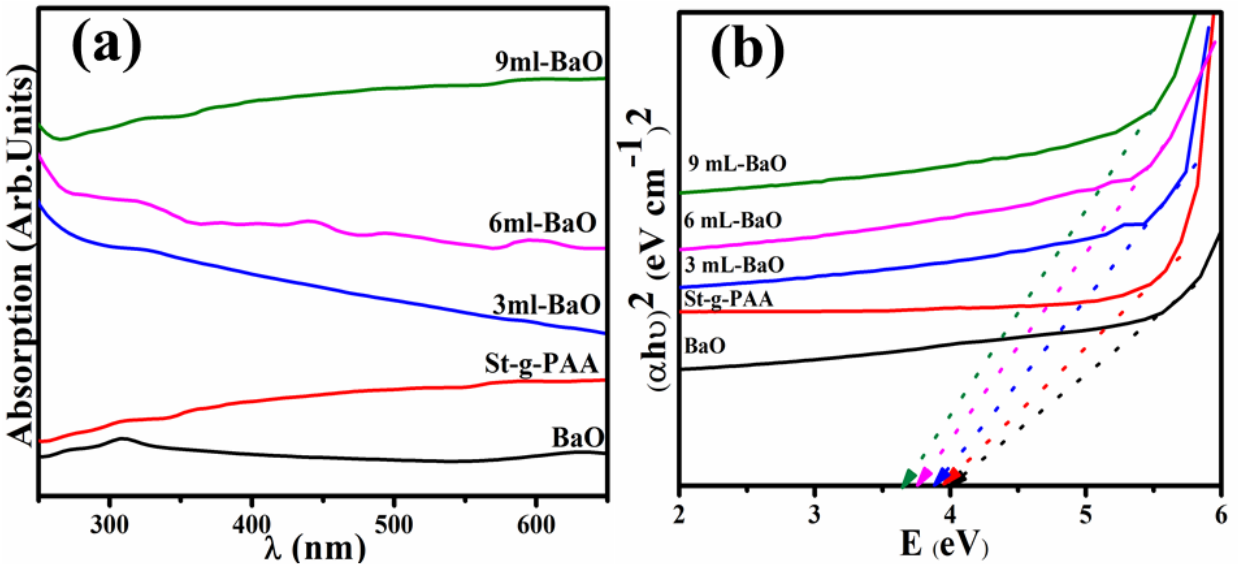

Fig. 4 (a) Electronic spectra and (b) band gap energy of BaO, St-g-PAA, and doped BaO

EDS was deployed to determine the constituent components of prepared samples, as shown in Fig 5(a-d). The existence of Ba and O peaks verified the creation of BaO. Additional peaks of Na was detected in all samples attributed to utilizing NaOH to sustain the pH during catalyst synthesis [39]. Au peak was detected due to the coating of Au sprayed over prepared materials to reduce charging influence [40]. Peak of K was seen in (Fig. 5b) as a precursor K_2SO_4 used to prepare St-g-PAA.

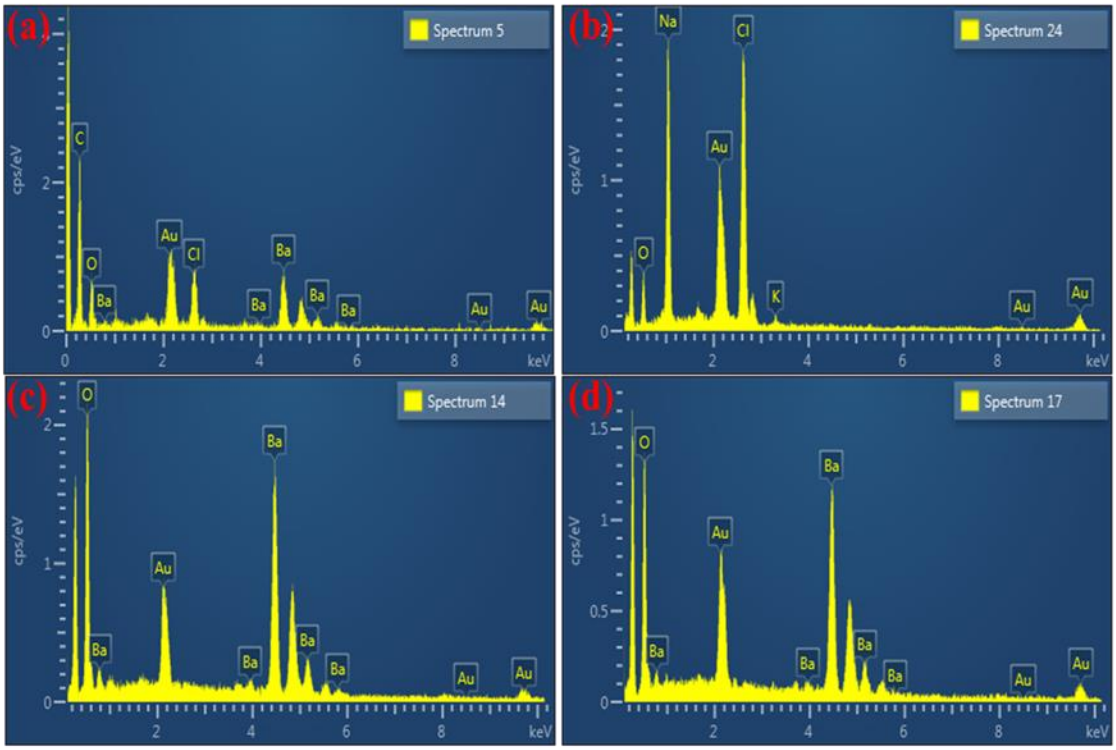

Fig. 5(a) EDS spectra of BaO (b) BaO-St-g-PAA (3,6, and 9mL) doped BaO, respectively.

Fig. 6(a-d) demonstrates the FESEM images of BaO, St-g-PAA, and doped BaO. BaO showed a chunk-like structure with unequal small-sized NPs, as shown in Fig. 6(a). Upon doping of St-g-PAA, a rod-shaped structure was observed that interacts with NPs, as demonstrated in Fig. 6(b). The diameter of nanorods was increased upon the higher concentration of St-g-PAA, as illustrated in Fig. 6(c-d).

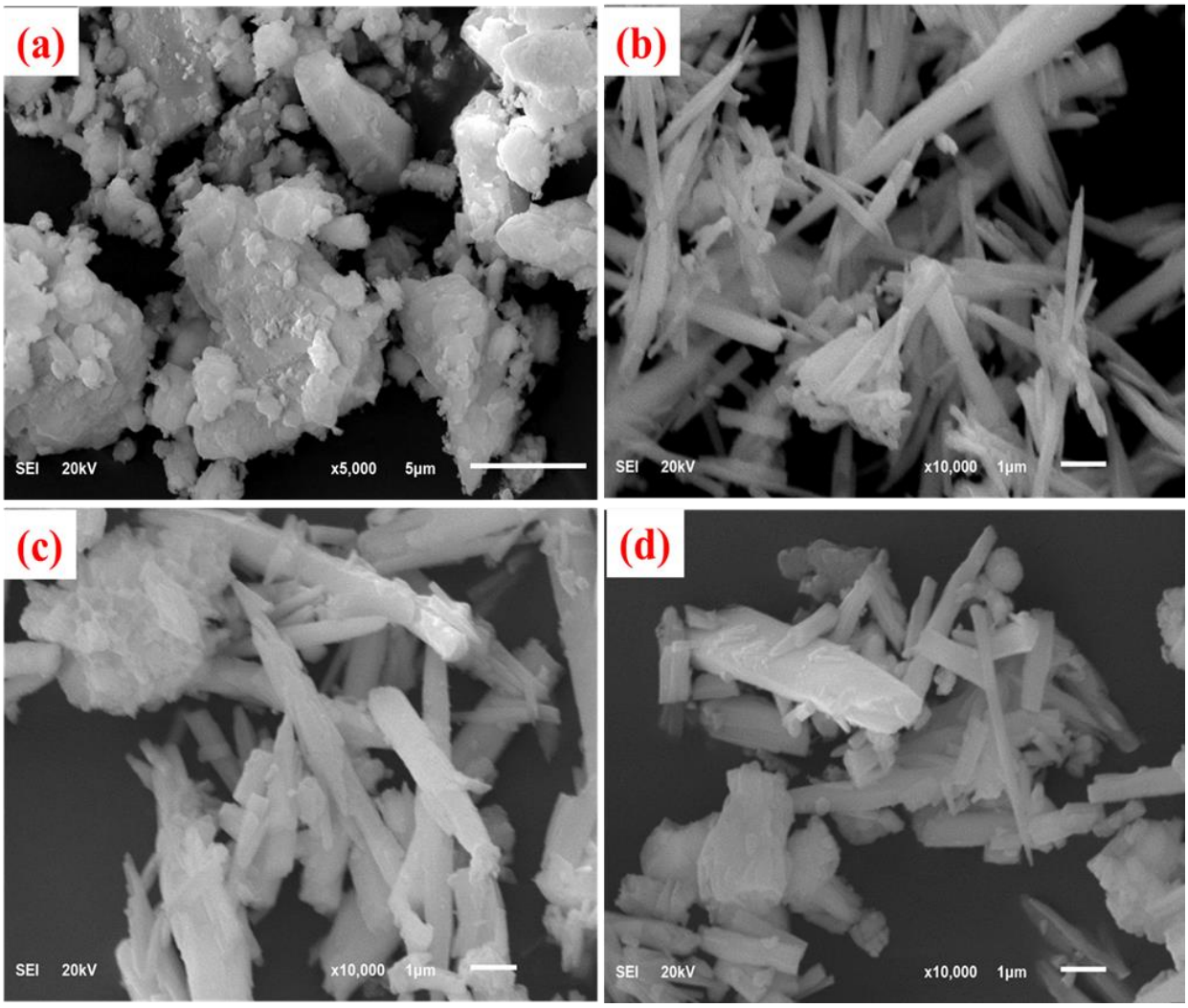

Fig. 6 (a-d) SEM analysis of BaO and St-g-PAA (3, 6, and 9 mL) doped BaO, respectively.

TEM was utilized to additional characterize the morphology and microstructure of pure and St-g-PAA-doped BaO NPs. The cubic-shaped morphology of BaO NPs is deliberated in Fig. 7(a). Fig. 7(b) demonstrates the high agglomeration of overlapped NPs. The doped samples exhibited a rod-like morphology that partially overlapped with NPs, as represented in Fig. 7(b-d). Interlayer spacing of BaO, St-g-PAA, and St-g-PAA doped BaO (3 and 6 mL) was calculated from a plane (101) as 0.17, 0.29, 0.32 and 0.22 nm, correspondingly that is well matched with XRD data as shown in Fig. 7(á-d´).

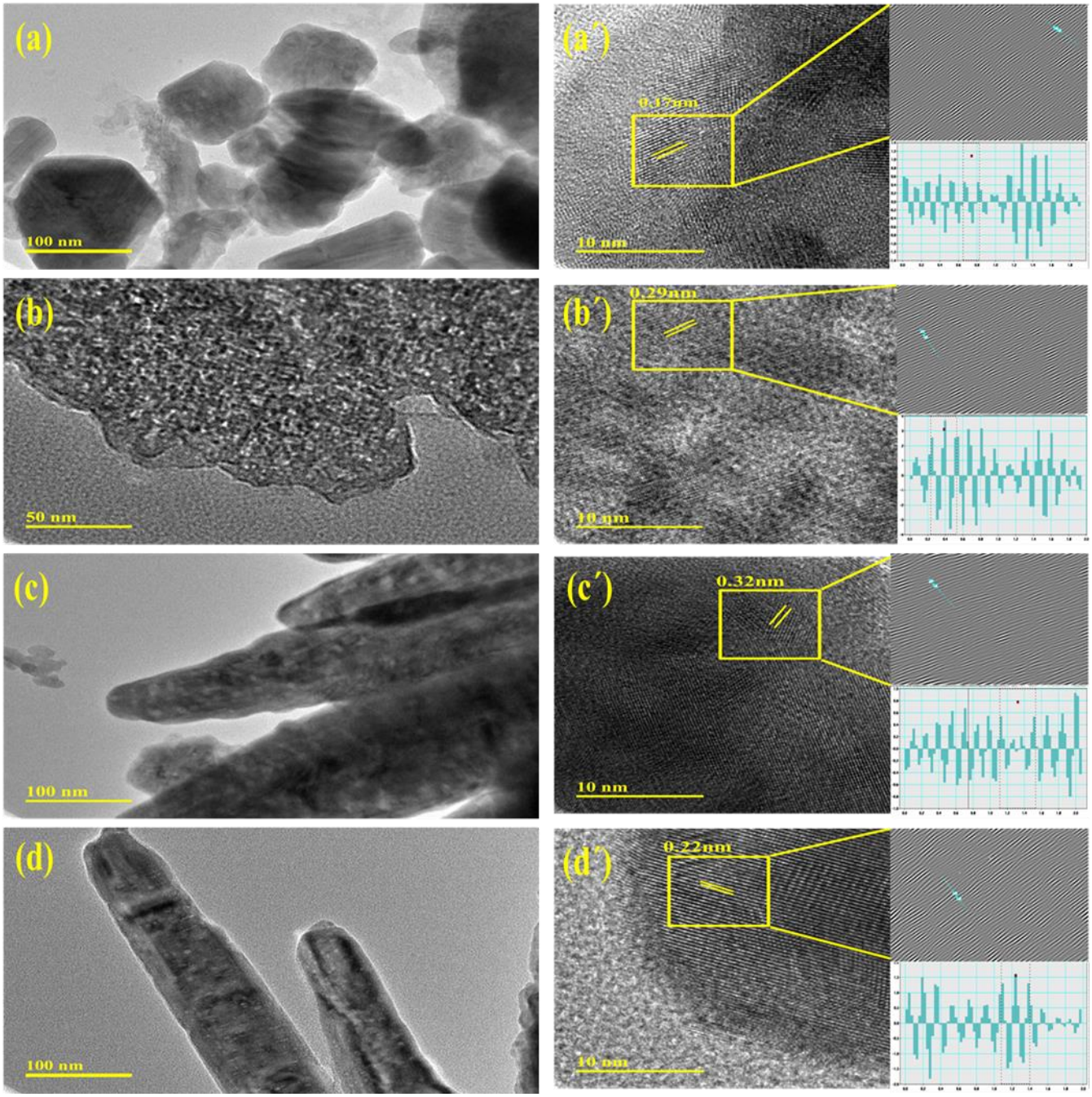

Fig. 7 (a-d) HR-TEM micrographs and, (á-d´) d-spacing of pure, St-g-PAA, and St-g-PAA (3 and 6 mL) doped BaO.

CA of pure, grafted, and doped BaO NPs in the occurrence of $NaBH_4$ for MB reduction was examined through a UV-Vis spectrophotometer. All samples explored maximum reduction of MB 61.6-75.1% in a neutral environment (pH~7), 67.8-79.9% in an acidic environment

(pH~3.5), and 61.7-97.6% in basic condition (pH~11.5) as demonstrated in Fig. 8(a-c), correspondingly. The crystal structure, particle size, and shape of the synthesized catalyst influenced the CA. Synthesized materials in the existence of $NaBH_4$ function as electron relays which shift the electron from BH_4^- to dye, causing the de-colorization of MB. NPs showed significant active sites that elevate the adsorption of MB and BH_4^-, which promotes the dye reduction efficacy. In an acidic environment, maximum reduction for 9 mL doped BaO attributed to a larger production of H^+ ion on catalyst surface. CA in a basic environment showed good results because of higher electrostatic interaction among negatively charged catalyst and positively charged MB dye. In a basic medium, catalysts get a negative charge on their surface, while the reduction of cationic MB in an acidic environment is hindered by positively charged catalyst surface [41] [42].

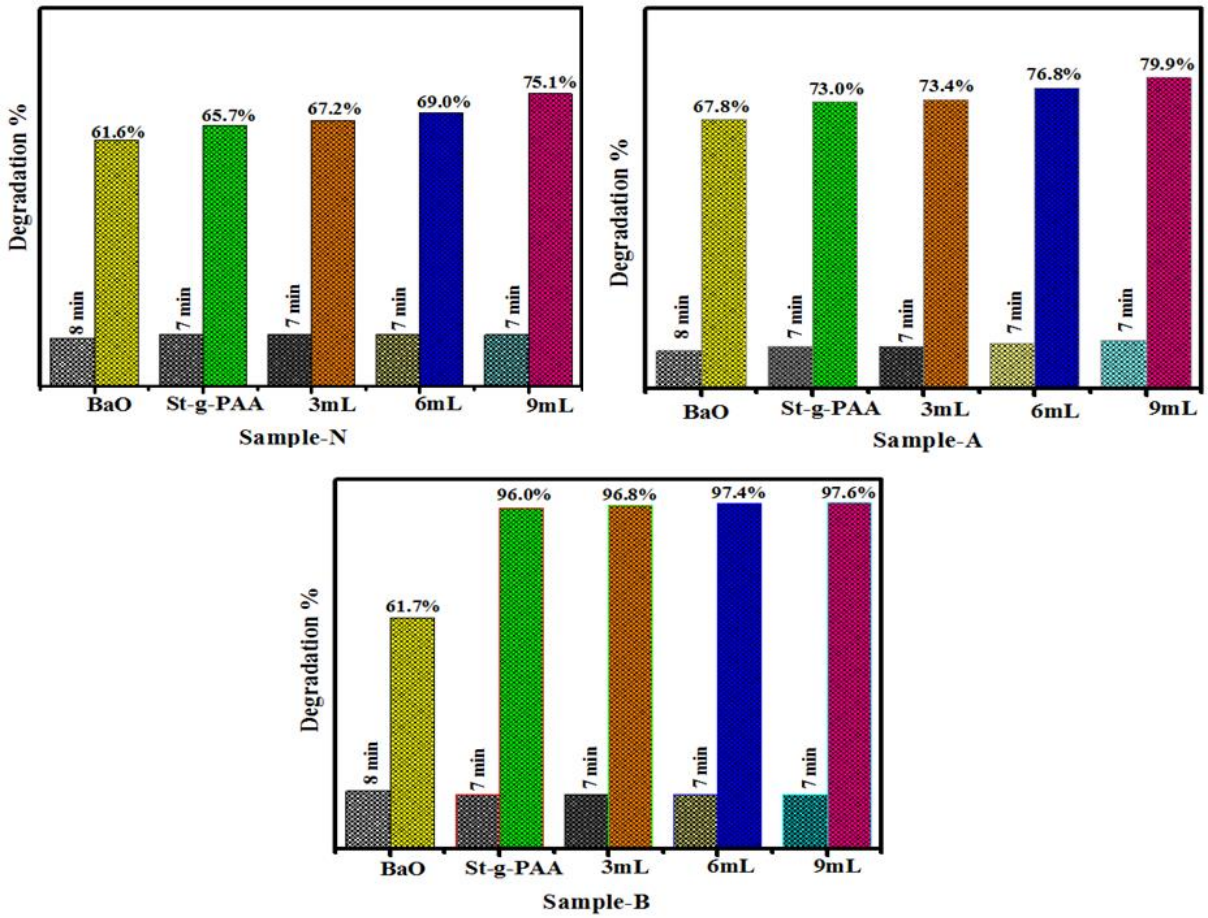

Fig. 8 Catalysis of BaO and St-g-PAA doped BaO (a) in neutral (b) Acidic and (c) Basic

3.1 Antimicrobial Activity

Antimicrobial performance of pure, St-g-PAA, and incorporated BaO were conducted by utilizing a well diffusion approach contrary to *S.aureus* and *E.coli* as represented in Table 1. At high concentrations, substantial inhibition zones ($P < 0.05$) for G ±ve were confirmed as (1.55 – 2.40 mm) for *E. coli* and (3.15-7.35 mm) for *S. aureus*, respectively. In contrast to DI water (0 mm), ciprofloxacin had an inhibition zone of 4.25 and 9.20 mm beside *E. coli* and *S. aureus*, correspondingly. In contrast to *E.coli*, synthesized NPs exhibited an increased antibacterial efficacy against *S. aureus* because cell wall of G -ve is thicker consisting large complex structure

than G +ve bacteria. The antibacterial efficacy of NPs assigned to different factors, including electrostatic relations of OH and H_2O_2 on the surface, which produce the reactive oxygen species (ROS) as demonstrated in Fig. 9. This caused the oxidative stress on bacteria's cell walls, resulting in the death of cells [43]. According to experimental findings, St-g- PAA dopant enhances BaO's antibacterial activity against *S. aureus* bacteria [18].

Table 1 Antimicrobial activity of St-g-PAA doped BaO

Samples	[1]Inhibition zone (mm)		[2]Inhibition zone (mm)	
	0.5mg/50µL	1.0mg/50µL	0.5mg/50µL	1.0mg/50µL
BaO	0	0	0	0
St-g-PAA	0	0	0	0
(3 mL)St-g-PAA: BaO	0	3.15	0	0
(6 mL)St-g-PAA:BaO	0	6.05	0	1.55
(9 mL)St-g-PAA:BaO	0	7.35	0	2.40
Ciprofloxacin	9.20	9.20	4.25	4.25
DIW	0	0	0	0

[1] Inhibition zones for *S.aureus*

[2] Inhibition zones for *E.coli*

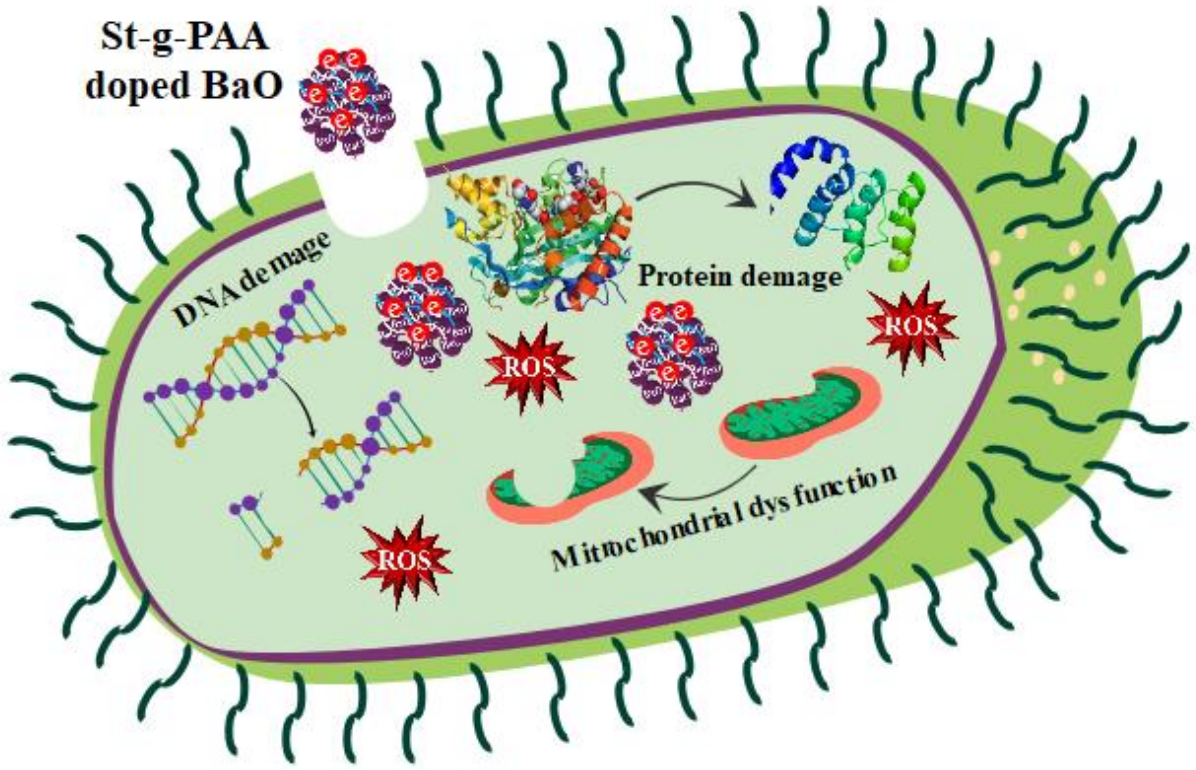

Fig. 9 Antibacterial mechanism of St-g-PAA doped BaO.

3.2 Molecular docking studies:

The role of nanoparticles as potential bactericidal agents have been extensively reported still the mystery behind this potency needs to be explored. Disruption of various cell processes by inhibiting enzyme targets has been considered an effective strategy for exploring new antibacterial agents [6,10]. Computational techniques represent a valuable source to predict possible mechanisms governing these biological activities, particularly molecular docking predictions [44,45]. In the case of FabI$_{S.\ aureus}$, both st-g-PAA and St-g-PAA doped BaO nanocomposites revealed good binding scores of -7.923 kcal/mol and -6.057 kcal/mol, respectively. Four H-bonds, i.e., Gly13 (2.7Å), Arg40 (2.6 Å), Ala95 (2.8 Å), Ser197 (2.7 Å), and two hydrophobic interactions with Ala15 and Ile94 served as main contributor towards the docked complex formation of st-g-PAA nanocomposite (Fig. 10A). Similarly, St-g-PAA doped

BaO nanocomposite complex with FabI$_{S.\ aureus}$ showed involvement of multiple H-bonds like Gly191 (3.1 Å), Thr195 (1.9 Å), and Ser197 (2.6 Å) alongside hydrophobic interactions with Ile20 and Thr145 as depicted in Fig. 10 B. On the contrary, docked complexes formed inside the active pocket of FabI$_{E.coli}$ showed differences in binding approach of st-g-PAA and St-g-PAA doped BaO nanocomposites. A docked complex formed in case of St-g-PAA doped BaO nanocomposites showed involvement of hydrophobic interactions as main factor for binding along with two H-bonds, i.e., Ser91 (3.0 Å) and Tyr156 (2.7 Å) having binding score -5.919 kcal/mol. On the other hand, st-g-PAA nanocomposite docked complex revealed multiple H-bonds like Ala21 (3.4 Å), Gly13 (3.0 Å), Ser19 (2.6 Å) and Lys163 (2.7 Å) along with hydrophobic interaction to Ile20 as shown in Figure 10 C & D.

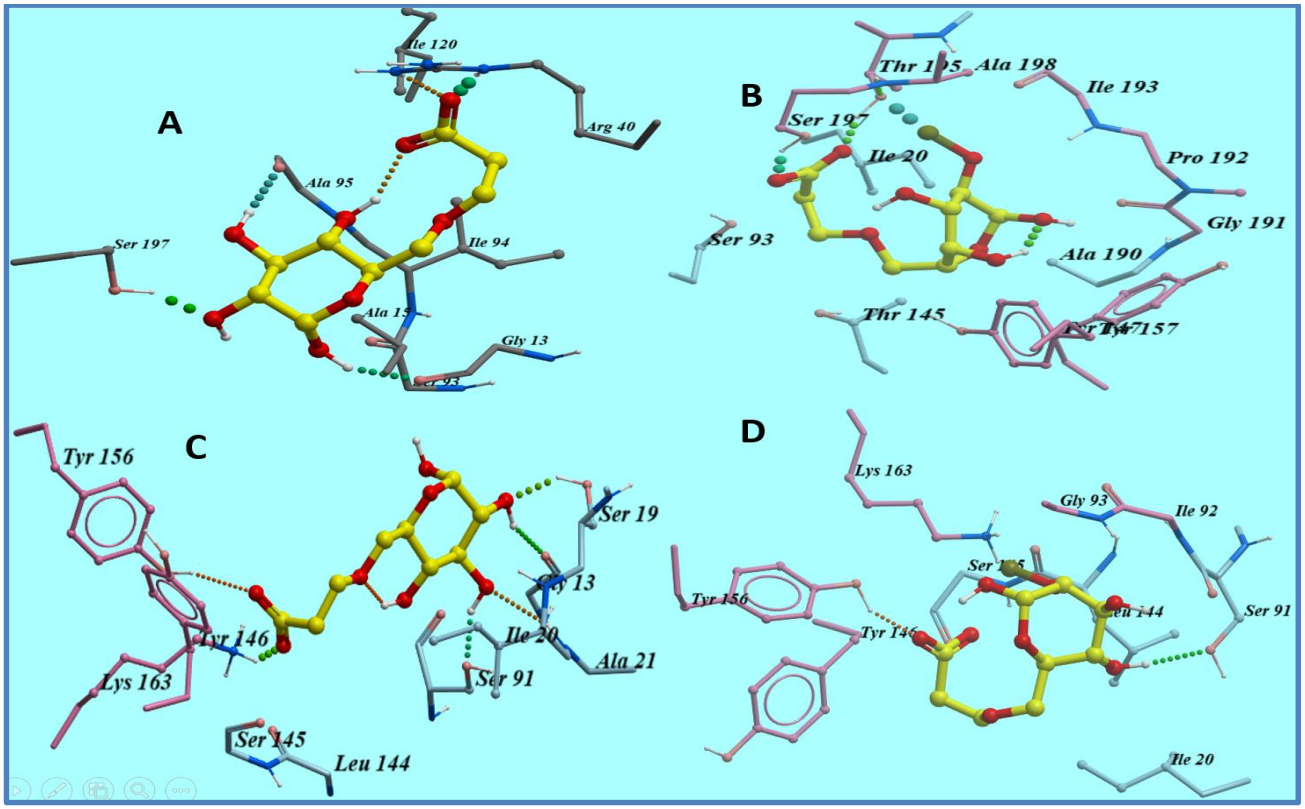

Fig. 10 Graphical representation of binding site interactions of FabI for St-g-PAA and St-g-PAA doped BaO nanocomposite A & B from *S. aureus* and C & D from *E. coli*

The second enzyme target selected was beta-lactamase, which is essential for bacterial survival and previously reported as an important target for discovering new antibiotics. Both these nanocomposites St-g-PAA and St-g-PAA doped BaO were evaluated for their binding mode and docked complex formation tendency within active site of beta lactamase$_{S.\ aureus}$. St-g-PAA showed three H-bond interactions with Ser403 (3.0 Å), Thr600 (2.9 Å), and Lys597 (3.3 Å), while Tyr446 and Ser462 were involved in hydrophobic interactions with a binding score as -5.598 kcal/mol. Similarly, four H-bonds were observed for St-g-PAA doped BaO nanocomposite docked complex as Asn464 (3.3 Å), His583 (2.6 Å), Ser598 (2.8 Å) and Thr600 (2.8 Å) along with pi-pi interaction with Tyr446 and other hydrophobic interactions (Fig. 11A & B). The binding score observed for St-g-PAA doped BaO nanocomposite-beta lactamase$_{S.\ aureus}$ docked complex was -9.101 kcal/mol.

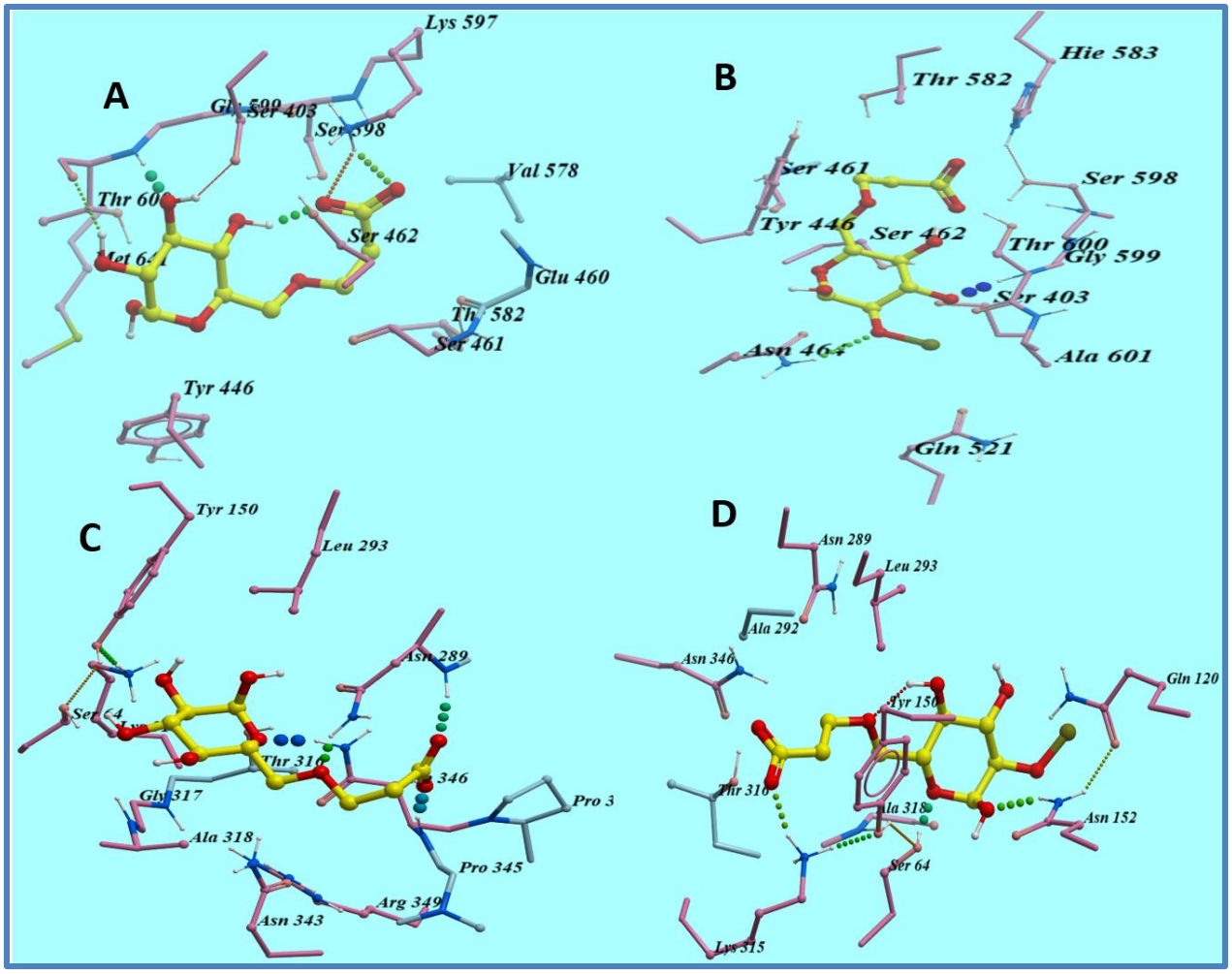

Fig. 11 Graphical representation of binding site interactions of beta-lactamase for St-g-PAA and St-g-PAA doped BaO nanocomposite A & B from *S. aureus* and C & D from *E. coli*

Also, in the case of St-g-PAA docked complex with beta lactamase$_{E.\ coli}$, Tyr150 revealed pi-pi interaction while Asn289 and Asn346 formed H-bonds having distances of 2.2 Å and 2.5 Å, respectively, with a score of -6.696 kcal/mol. St-g-PAA doped BaO nanocomposite showed similar binding patterns like the involvement of pi-pi correlation with Tyr150 and three H-bonds as Ser64 (2.5 Å), Asn152 (2.9 Å), Lys315 (2.7 Å) along with hydrophobic relation with Lys293 having docking score -7.783 kcal/mol (Fig 11C & D).

4 CONCLUSION

In order to determine the antibacterial and catalytic activity, different concentrations of St-g-PAA doped BaO NPs were effectively produced by a simple co-precipitation method. BaO has tetragonal structure confirmed by the XRD pattern, which showed that reduction in crystallinity upon dopants. FTIR was used to confirm the occurrence of functional groups in prepared NPs and polycrystalline nature of BaO was validated through SAED. According to UV-Vis spectra, doping caused to decrease the bandgap energy from 4.00 to 3.79 eV. The d-spacing (0.17, 0.29, 0.32, and 0.22 nm) was calculated using HR-TEM, which correlates with XRD. The maximum catalytic degradation of MB was observed at 97% for doped samples in a basic environment. Additionally, the bactericidal efficacy of the BaO NPs was determined against the bacteria *S. aureus* and *E. coli* (0-2.40 mm)*;* while higher antibacterial performance was observed by the *S. aureus* (0-7.35 mm) at higher concentration compared to and *E. coli* (0-2.40 mm) upon doping. In silico studies were carried out against enoyl-[acylcarrier-protein] reductase (FabI) and beta-lactamase enzyme to assess St-g-PAA and St-g-PAA doped BaO nanocomposites as inhibitors and elucidates their mode of action. From these results, we conclude that St-g-PAA doped BaO NPs can be used as ideal catalyst in basic media and potential inhibitor.

Acknowledgment: Thanks to higher education commission (HEC), Pakistan for NRPU-20-17615 (Muhammad Ikram).

REFERENCES

[1] M.M. Hasan, M.A. Shenashen, M.N. Hasan, H. Znad, M.S. Salman, M.R. Awual, Natural biodegradable polymeric bioadsorbents for efficient cationic dye encapsulation from wastewater, J. Mol. Liq. 323 (2021). https://doi.org/10.1016/j.molliq.2020.114587.

[2] S. Moniri Javadhesari, S. Alipour, S. Mohammadnejad, M.R. Akbarpour, Antibacterial activity of ultra-small copper oxide (II) nanoparticles synthesized by mechanochemical processing against S. aureus and E. coli, Mater. Sci. Eng. C. 105 (2019). https://doi.org/10.1016/j.msec.2019.110011.

[3] R.N. Bharagava, G. Saxena, S.I. Mulla, Introduction to Industrial Wastes Containing Organic and Inorganic Pollutants and Bioremediation Approaches for Environmental Management, in: Bioremediation Ind. Waste Environ. Saf., Springer Singapore, 2020: pp. 1–18. https://doi.org/10.1007/978-981-13-1891-7_1.

[4] A. Raza, M. Ikram, M. Aqeel, M. Imran, A. Ul-Hamid, K.N. Riaz, S. Ali, Enhanced industrial dye degradation using Co doped in chemically exfoliated MoS2 nanosheets, Appl. Nanosci. 10 (2020) 1535–1544. https://doi.org/10.1007/s13204-019-01239-3.

[5] M.M. Ghangrekar, P. Chatterjee, Water pollutants classification and its effects on environment, in: Carbon Nanostructures, Springer International Publishing, 2018: pp. 11–26. https://doi.org/10.1007/978-3-319-95603-9_2.

[6] M. Ikram, A. Mahmood, A. Haider, S. Naz, A. Ul-Hamid, W. Nabgan, I. Shahzadi, J. Haider, I. Ahmad, S. Ali, Dye degradation, antibacterial and in-silico analysis of Mg/cellulose-doped ZnO nanoparticles, Int. J. Biol. Macromol. 185 (2021) 153–164. https://doi.org/10.1016/j.ijbiomac.2021.06.101.

[7] B.C. Hodges, E.L. Cates, J.H. Kim, Challenges and prospects of advanced oxidation water treatment processes using catalytic nanomaterials, Nat. Nanotechnol. 13 (2018) 642–650. https://doi.org/10.1038/s41565-018-0216-x.

[8] M. Rafatullah, O. Sulaiman, R. Hashim, A. Ahmad, Adsorption of methylene blue on low-cost adsorbents: A review, J. Hazard. Mater. 177 (2010) 70–80. https://doi.org/10.1016/j.jhazmat.2009.12.047.

[9] M.D.A. Khan, A. Akhtar, S.A. Nabi, M.A. Khan, Synthesis, characterization, and photocatalytic activity of polyaniline-Sn(IV)iodophosphate nanocomposite: Its application in wastewater detoxification, Ind. Eng. Chem. Res. 53 (2014) 15253–15260. https://doi.org/10.1021/ie502804s.

[10] A. Rafiq, M. Ikram, S. Ali, F. Niaz, M. Khan, Q. Khan, M. Maqbool, Photocatalytic degradation of dyes using semiconductor photocatalysts to clean industrial water pollution, J. Ind. Eng. Chem. 97 (2021) 111–128. https://doi.org/10.1016/j.jiec.2021.02.017.

[11] M. Serhan, M. Sprowls, D. Jackemeyer, M. Long, I.D. Perez, W. Maret, N. Tao, E. Forzani, Total iron measurement in human serum with a smartphone, in: AIChE Annu. Meet. Conf. Proc., 2019: pp. 1–3. https://doi.org/10.1039/x0xx00000x.

[12] A. Arshad, J. Iqbal, M. Siddiq, M.U. Ali, A. Ali, H. Shabbir, U. Bin Nazeer, M.S. Saleem, Solar light triggered catalytic performance of graphene-CuO nanocomposite for waste water treatment, Ceram. Int. 43 (2017) 10654–10660. https://doi.org/10.1016/j.ceramint.2017.03.165.

[13] H. Wang, J.Z. Xu, J.J. Zhu, H.Y. Chen, Preparation of CuO nanoparticles by microwave irradiation, J. Cryst. Growth. 244 (2002) 88–94. https://doi.org/10.1016/S0022-0248(02)01571-3.

[14] F. Naz, K. Saeed, Synthesis of barium oxide nanoparticles and its novel application as a catalyst for the photodegradation of malachite green dye, Appl. Water Sci. 12 (2022). https://doi.org/10.1007/s13201-022-01649-9.

[15] R. Gillani, B. Ercan, A. Qiao, T.J. Webster, Nanofunctionalized zirconia and barium sulfate particles as bone cement additives, Int. J. Nanomedicine. 5 (2010) 1–11. https://doi.org/10.2147/ijn.s7603.

[16] M.S. Mauter, I. Zucker, F. Perreault, J.R. Werber, J.H. Kim, M. Elimelech, The role of nanotechnology in tackling global water challenges, Nat. Sustain. 1 (2018) 166–175. https://doi.org/10.1038/s41893-018-0046-8.

[17] A. Biswal, P.K. Sethy, S.K. Swain, Change in Orientation of Polyacrylic Acid and Chitosan Networks by Imprintment of Gold Nanoparticles, Polym. Technol. Mater. 60 (2021) 182–194. https://doi.org/10.1080/25740881.2020.1793196.

[18] F. Jamal, M. Ikram, A. Haider, A. Ul-Hamid, M. Ijaz, W. Nabgan, J. Haider, I. Shahzadi, Facile synthesis of silver and polyacrylic acid doped magnesium oxide nanostructure for photocatalytic dye degradation and bactericidal behavior, Appl. Nanosci. 12 (2022) 2409–2419. https://doi.org/10.1007/s13204-022-02504-8.

[19] Y. Tang, Y. Li, Y. Zhang, C. Mu, J. Zhou, W. Zhang, B. Shi, Nonswelling Silica-Poly(acrylic acid) Composite for Efficient and Simultaneous Removal of Cationic Dye, Heavy Metal, and Surfactant-Stabilized Emulsion from Wastewater, Ind. Eng. Chem. Res. 59 (2020) 3383–3393. https://doi.org/10.1021/acs.iecr.9b05120.

[20] A. Saberi, E. Alipour, M. Sadeghi, Superabsorbent magnetic Fe3O4-based starch-poly

(acrylic acid) nanocomposite hydrogel for efficient removal of dyes and heavy metal ions from water, J. Polym. Res. 26 (2019). https://doi.org/10.1007/s10965-019-1917-z.

[21] M.R. Shaik, M. Kuniyil, M. Khan, N. Ahmad, A. Al-Warthan, M.R.H. Siddiqui, S.F. Adil, D.J. McPhee, Modified polyacrylic acid-zinc composites: Synthesis, characterization and biological activity, Molecules. 21 (2016). https://doi.org/10.3390/molecules21030292.

[22] L. Boels, G.J. Witkamp, Carboxymethyl inulin biopolymers: A green alternative for phosphonate calcium carbonate growth inhibitors, Cryst. Growth Des. 11 (2011) 4155–4165. https://doi.org/10.1021/cg2007183.

[23] M. Ikram, S. Hayat, M. Imran, A. Haider, S. Naz, A. Ul-Hamid, I. Shahzadi, J. Haider, A. Shahzadi, W. Nabgan, S. Ali, Novel Ag/cellulose-doped CeO2 quantum dots for efficient dye degradation and bactericidal activity with molecular docking study, Carbohydr. Polym. 269 (2021). https://doi.org/10.1016/j.carbpol.2021.118346.

[24] S. Shaheen, A. Iqbal, M. Ikram, K. Ul-Ain, S. Naz, A. Ul-Hamid, A. Shahzadi, A. Haider, W. Nabgan, J. Haider, Effective Disposal of Methylene Blue and Bactericidal Benefits of Using GO-Doped MnO2Nanorods Synthesized through One-Pot Synthesis, ACS Omega. 6 (2021) 24866–24878. https://doi.org/10.1021/acsomega.1c03723.

[25] N. Bahadoran Baghbadorani, T. Behzad, M.H. Karimi Darvanjooghi, N. Etesami, Modelling of water absorption kinetics and biocompatibility study of synthesized cellulose nanofiber-assisted starch-graft-poly(acrylic acid) hydrogel nanocomposites, Cellulose. 27 (2020) 9927–9945. https://doi.org/10.1007/s10570-020-03511-0.

[26] M.A. Ansari, N. Jahan, Structural and Optical Properties of BaO Nanoparticles

Synthesized by Facile Co-precipitation Method, Mater. Highlights. 2 (2021) 23. https://doi.org/10.2991/mathi.k.210226.001.

[27] S.M. Drawz, R.A. Bonomo, Three decades of β-lactamase inhibitors, Clin. Microbiol. Rev. 23 (2010) 160–201. https://doi.org/10.1128/CMR.00037-09.

[28] J. Schiebel, A. Chang, S. Shah, Y. Lu, L. Liu, P. Pan, M.W. Hirschbeck, M. Tareilus, S. Eltschkner, W. Yu, J.E. Cummings, S.E. Knudson, G.R. Bommineni, S.G. Walker, R.A. Slayden, C.A. Sotriffer, P.J. Tonge, C. Kisker, Rational design of broad spectrum antibacterial activity based on a clinically relevant enoyl-acyl carrier protein (ACP) reductase inhibitor, J. Biol. Chem. 289 (2014) 15987–16005. https://doi.org/10.1074/jbc.M113.532804.

[29] J. Schiebel, A. Chang, B. Merget, G.R. Bommineni, W. Yu, L.A. Spagnuolo, M. V Baxter, M. Tareilus, P.J. Tonge, C. Kisker, C.A. Sotriffer, An Ordered Water Channel in Staphylococcus aureus FabI: Unraveling the Mechanism of Substrate Recognition and Reduction, Biochemistry. 54 (2015) 1943–1955. https://doi.org/10.1021/bi5014358.

[30] D. Lim, N.C.J. Strynadka, Structural basis for the β-lactam resistance of PBP2a from methicillin-resistant Staphylococcus aureus, Nat. Struct. Biol. 9 (2002) 870–876. https://doi.org/10.1038/nsb858.

[31] S. Barelier, O. Eidam, I. Fish, J. Hollander, F. Figaroa, R. Nachane, J.J. Irwin, B.K. Shoichet, G. Siegal, Increasing chemical space coverage by combining empirical and computational fragment screens, ACS Chem. Biol. 9 (2014) 1528–1535. https://doi.org/10.1021/cb5001636.

[32] R. Abagyan, M. Totrov, Biased probability Monte Carlo conformational searches and electrostatic calculations for peptides and proteins, J. Mol. Biol. 235 (1994) 983–1002. https://doi.org/10.1006/jmbi.1994.1052.

[33] A.Z. Bazeera, M.I. Amrin, Synthesis and Characterization of Barium Oxide Nanoparticles, IOSR J. Appl. Phys. 01 (2017) 76–80. https://doi.org/10.9790/4861-17002017680.

[34] O.A. Bin-Dahman, J. Jose, M.A. Al-Harthi, Compatibility of poly(acrylic acid)/starch blends, Starch/Staerke. 67 (2015) 1061–1069. https://doi.org/10.1002/star.201500011.

[35] N. C, Y. K V, M.P. R, S. M, G.B. R, Simultaneous refining of biodiesel-derived crude glycerol and synthesis of value-added powdered catalysts for biodiesel production: A green chemistry approach for sustainable biodiesel industries, J. Clean. Prod. 363 (2022). https://doi.org/10.1016/j.jclepro.2022.132448.

[36] M. Ikram, N. Abid, A. Haider, A. Ul-Hamid, J. Haider, A. Shahzadi, W. Nabgan, S. Goumri-Said, A.R. Butt, M. Benali Kanoun, Toward efficient dye degradation and the bactericidal behavior of Mo-doped La2O3nanostructures, Nanoscale Adv. 4 (2022) 926–942. https://doi.org/10.1039/d1na00802a.

[37] A. Ashfaq, M. Ikram, A. Haider, A. Ul-Hamid, I. Shahzadi, J. Haider, Nitrogen and Carbon Nitride-Doped TiO2 for Multiple Catalysis and Its Antimicrobial Activity, Nanoscale Res. Lett. 16 (2021). https://doi.org/10.1186/s11671-021-03573-4.

[38] S. K K, A. Saji, A. Chanda, M. Vasundhara, Effects of Calcinations Temperatures on Structural, optical and magnetic properties of MgO nanoflakes and its photocatalytic

applications, Opt. Mater. (Amst). 132 (2022). https://doi.org/10.1016/j.optmat.2022.112777.

[39] M. Ikram, T. Inayat, A. Haider, A. Ul-Hamid, J. Haider, W. Nabgan, A. Saeed, A. Shahbaz, S. Hayat, K. Ul-Ain, A.R. Butt, Graphene Oxide-Doped MgO Nanostructures for Highly Efficient Dye Degradation and Bactericidal Action, Nanoscale Res. Lett. 16 (2021). https://doi.org/10.1186/s11671-021-03516-z.

[40] M. Ikram, S. Aslam, A. Haider, S. Naz, A. Ul-Hamid, A. Shahzadi, M. Ikram, J. Haider, S.O.A. Ahmad, A.R. Butt, Doping of Mg on ZnO Nanorods Demonstrated Improved Photocatalytic Degradation and Antimicrobial Potential with Molecular Docking Analysis, Nanoscale Res. Lett. 16 (2021). https://doi.org/10.1186/s11671-021-03537-8.

[41] L. Yang, X. Yang, R. Zhou, Probing BaO Doping Effect on the Structure and Catalytic Performance of Pd/CexZr1-xO2 (x = 0.2-0.8) Catalysts for Automobile Emission Control, J. Phys. Chem. C. 120 (2016) 2712–2723. https://doi.org/10.1021/ACS.JPCC.5B10301.

[42] A. Bari, M. Ikram, A. Haider, A. Ul-Hamid, J. Haider, I. Shahzadi, G. Nazir, A. Shahzadi, M. Imran, A. Ghaffar, Evaluation of bactericidal potential and catalytic dye degradation of multiple morphology based chitosan/polyvinylpyrrolidone-doped bismuth oxide nanostructures, Nanoscale Adv. 4 (2022) 2713–2728. https://doi.org/10.1039/d2na00105e.

[43] M. Ikram, A. Shahzadi, S. Hayat, W. Nabgan, A. Ul-Hamid, A. Haider, M. Noor, S. Goumri-Said, M.B. Kanoun, S. Ali, Novel Ta/chitosan-doped CuO nanorods for catalytic purification of industrial wastewater and antimicrobial applications, RSC Adv. 12 (2022) 16991–17004. https://doi.org/10.1039/d2ra03006c.

[44] D. Seeliger, B.L. De Groot, Ligand docking and binding site analysis with PyMOL and Autodock/Vina, J. Comput. Aided. Mol. Des. 24 (2010) 417–422. https://doi.org/10.1007/s10822-010-9352-6.

[45] M.N. Mohamad Rosdi, S. Mohd Arif, M.H. Abu Bakar, S.A. Razali, R. Mohamed Zulkifli, H. Ya'akob, Molecular docking studies of bioactive compounds from Annona muricata Linn as potential inhibitors for Bcl-2, Bcl-w and Mcl-1 antiapoptotic proteins, Apoptosis. 23 (2018) 27–40. https://doi.org/10.1007/s10495-017-1434-7.

Assessment of Catalytic, Antimicrobial and Molecular Docking Analysis of Starch-Grafted Polyacrylic Acid Doped BaO Nanoparticles

Muhammad Ikram[a*], Ali Haider[b], Muhammad Imran[c], Junaid Haider[d], Sadia Naz[d], Anwar Ul-Hamid[e], Anum Shahzadi[f], Kinza Ghazanfar[g], Walid Nabgan[h*], Sawaira Moeen[a], Salamat Ali[g]

[a]Solar Cell Applications Research Lab, Department of Physics, Government College University Lahore, 54000, Pakistan

[b]Department of Clinical Sciences, Faculty of Veterinary and Animal Sciences, Muhammad Nawaz Shareef University of Agriculture, Multan, 66000, Pakistan

[c]Department of Chemistry, Government College University Faisalabad, Pakpattan Road, Sahiwal, Punjab, 57000, Pakistan

[d]Tianjin Institute of Industrial Biotechnology, Chinese Academy of Sciences, Tianjin 300308, China.

[e]Core Research Facilities, King Fahd University of Petroleum & Minerals, Dhahran, 31261, Saudi Arabia

[f]Faculty of Pharmacy, The University of Lahore, Lahore, 54000, Pakistan

[g]Department of Physics, Riphah Institute of Computing and Applied Sciences (RICAS), Riphah International University, 14 Ali Road, Lahore, Pakistan

[h]Departament d'Enginyeria Química, Universitat Rovira i Virgili, Av Països Catalans 26, 43007 Tarragona, Spain

*Corresponding author email: [a]dr.muhammadikram@gcu.edu.pk, [h]wnabgan@gmail.com

ABSTRACT

The removal of cationic dyes from water has received a great attention of researchers considering their influence on environment and ecosystem. In current work, starch-grafted-poly acrylic acid (St-g-PAA) doped BaO nanoparticles have been synthesized by co-precipitation approach. The aim of this research was to reduce the harmful methylene blue dye and evaluate the antibacterial activity of St-g-PAA doped BaO. XRD spectra exhibited the tetragonal structure of BaO and no variations occurred upon doping. The optical properties of St-g-PAA doped BaO have been evaluated by UV–Vis spectrophotometer. The existence of a dopant in the product was verified using EDS spectroscopy. TEM revealed the formation of cubic-shaped NPs of BaO and upon the addition of St-g-PAA, a few nanorod-like structures. The higher concentration of St-g-PAA doped BaO exhibit a remarkable reduction of methylene blue in a basic environment. Furthermore, St-g-PAA doped BaO revealed higher antimicrobial efficacy against *Staphylococcus aureus* in comparison to *Escherichia coli*. *In silico* studies were conducted against enoyl-[acylcarrier-protein] reductase (FabI) and beta-lactamase enzyme to evaluate the potential of both St-g-PAA and St-g-PAA doped BaO nanocomposites as their inhibitors and to rationalize their possible mode of action.

Keywords: Starch; BaO; catalysis

1. INTRODUCTION

Water is a basic component for the existence of the living organism. Only 0.03% of water on earth's surface is fresh, and it is found in water reservoirs like freshwater lakes and rivers [1]. Rapid urbanization and industrialization have a direct negative influence on the environment and human lives. Numerous industries regularly generate harmful dyes as waste products, including the leather, textiles, paper, cosmetics, and food industries [2–5]. Heavy metals and other organic

and inorganic contaminants, including phenols, dyes, polyaromatic hydrocarbons, pesticides, and mineral acids, are found in industrial wastewater along with sulphate, inorganic salts, and trace elements [2,6,7]. Pesticides used on farms, radioactive and industrial waste, marine dumping, and a deteriorating sewage system are all contributing factors that have made contamination a significant issue worldwide. The environment and human life are negatively and destructively affected by water contamination [2,8–10]. Methylene blue (MB), a cationic dye that is widely used in a variety of industries, including the production of paper, food processing, the fashion industry, and printing, has been identified as a concerning cause of water pollution.

Additionally, Gram-positive (G +ve) and Gram-negative (G-ve) microbes are examples of water-borne pathogens that can infect humans. The current state of affairs makes it a global challenge to ensure clean water, making the removal of dyes from aqueous media an essential element [4,11,12]. The impurities from industrial water have been removed using membrane filtering, reverse osmosis, photocatalysis, electrolysis, ion exchange, filtration process, , and microbial control [13].

One of these methods that play an important role in effectively reducing hazardous contaminants is catalysis. It is cost-effective, energy-efficient, and environmentally safe [4]. Transition metal oxides (TMO) are the semiconductor materials that finds numerous uses in photocatalytic degradation, and catalysis [14]. Due to their extensive study and varied applications, TMO, such as CuO, iron oxide, BaO, SnO_2, and ZnO are viewed as one of the wealthiest nanomaterial families [15]. Due to its wide band gap (4.4 eV) and hygroscopic properties, as well as its extensive applications in the fields of self-cleaning, pharmaceutical industry, electrical energy generation, and sensors, researchers have found great interest in BaO NPs [16]. Various

approaches have been used to synthesize BaO NPs with different sizes and shapes, as sol-gel, co-precipitation, and hydrothermal and thermal decomposition [17].

Among these techniques, the co-precipitation technique has gained attention in the industry due to its simple and direct synthesis, and energy-efficient and affordable approach for good yields and mass production [18]. Due to their low cost and ease of processing, polymers such as polyacrylic acid, and polyvinyl pyrrolidone (PVP), among others, have been extensively utilized as dopants [19]. Because of the existence of the carboxyl group, PAA demonstrated a significant capability for the reduction of heavy metal ions and MB from polluted water, along with high antibacterial efficacy. Additionally, PAA based-Nano composites (PAA-TiO_2) have been widely used in optical devices, solar cells, wastewater treatment, and protective covering [20–22]. A class of natural polymers called polysaccharides, including starch, chitosan, inulin, and alginate, are abundant in functional groups like hydroxyl, amino groups, and carboxyl, have favorable chelation and dispersion effects [23]. In recent biopolymer developments, natural polysaccharides have been emphasized as therapeutic agents. Starch and chitosan can be used as adsorbent materials in wastewater treatment because they are biodegradable and don't contain toxins [24]. Based on the above, we believe that using St-g-PAA-doped BaO nanoparticles (NPs) as a catalyst to remove wastewater are a viable option. Additionally, antibacterial activity of pristine and doped BaO NPs was also evaluated. *In silico*, docking studies were also performed to evaluate possible modes of action for both St-g-PAA and St-g-PAA doped BaO nanocomposites against given enzyme targets, i.e., enoyl-[acylcarrier-protein] reductase (FabI) and beta-lactamase from both *E. coli* and *S. aureus*. The synthesis of St-g-PAA-doped BaO oxide NPS was accomplished by the use of co-precipitation, which is a method that is simple, easy to reproduce, and inexpensive.

2. EXPERIMENTAL SECTION

2.1 Material Section

($BaCl_2$ $2H_2O$, 99%), sodium hydroxide (NaOH, 98.5%), starch ($C_6H_{10}O_5$), poly acrylic acid $(C_3H_4O_2)n$, and potassium sulphate (K_2SO_4).

2.2 Synthesis of Starch grafted polyacrylic acid

To synthesize starch-grafted polyacrylic acid, the desired amount of starch and acrylic acid (1:3) was added in 200 mL distilled water under vigorous stirring as elaborated in Fig. 1(a). 2 mg of potassium persulphate has been incorporated into the solution and stirred at 70 °C for 5 hours [25].

2.3 Synthesis of St-g-PAA doped BaO

To synthesize BaO NPs, $BaCl_2$. $2H_2O$ (0.5 M) was prepared under robust stirring at 90 °C for 30 minutes. Precipitating agent (NaOH) was integrated drop wise in above solution to sustain pH~ 12. Moreover, the stirred solution has been centrifuged at 7000 rpm and then dried at 160 °C overnight. The acquired BaO was crushed into fine powder. Similarly, different concentrations of St-g-PAA doped BaO were prepared by the cop-precipitation approach, as discussed earlier and demonstrated in Fig. 1(b) [26].

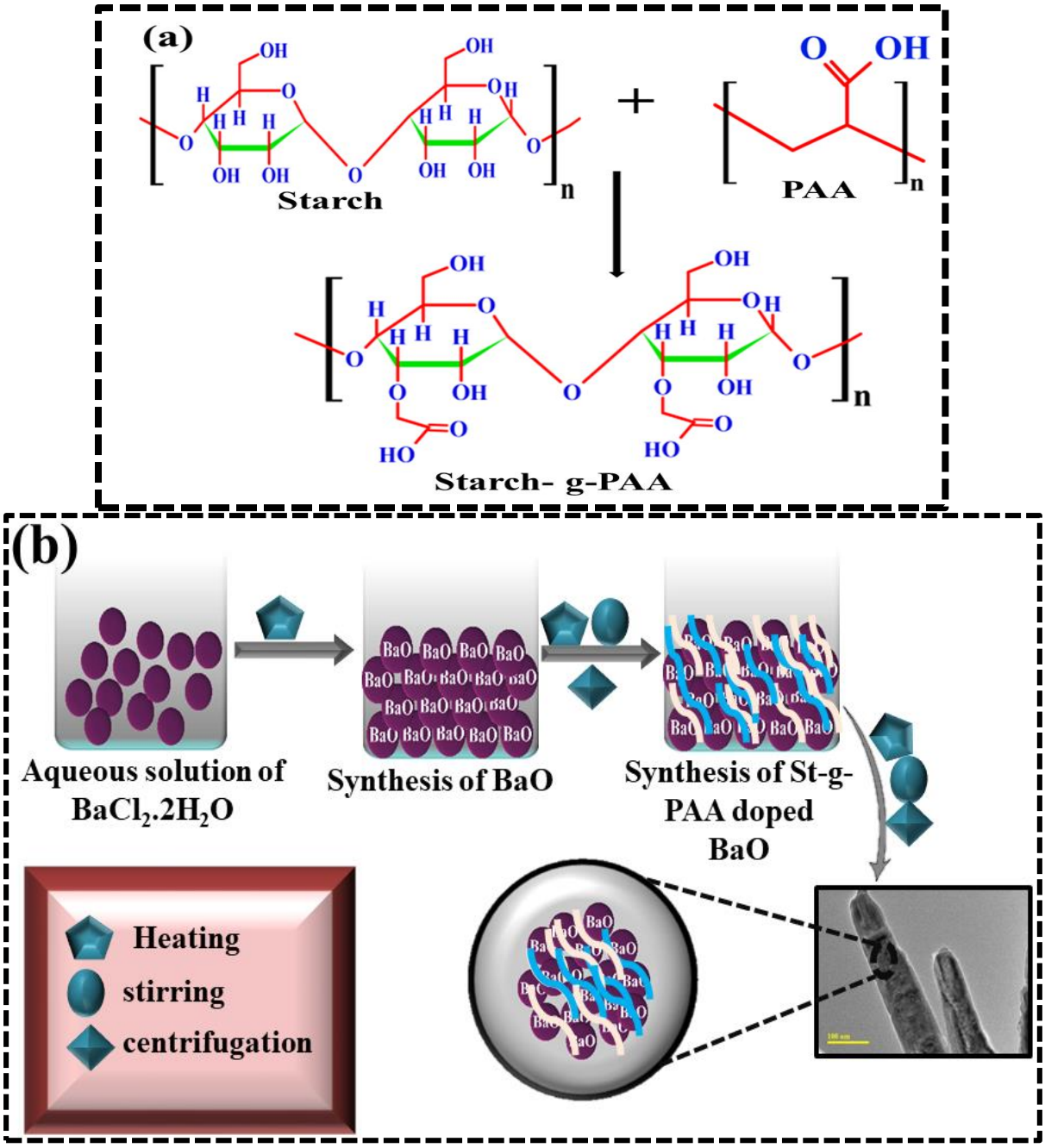

Fig.1 (a) Mechanism of St-g-PAA and (b) Synthesis of St-g-PAA doped BaO NPs

2.4 Catalytic Activity

The catalytic activity (CA) of BaO, St-g-PAA, and incorporated BaO NPs were examined by MB reduction in the existence of $NaBH_4$. The de-colorization of dye was observed at constant intervals by mixing the 400 µL $NaBH_4$ solution with 3mL MB solution. After that, 400 µL of

synthesized samples were incorporated and stirred at ambient temperature to above solution. UV-Vis spectrophotometer was operated to check the MB reduction efficacy in the wavelength range from 200-800 nm.

2.5 Catalysis mechanism

During CA, shifting an electron from $NaBH_4$ (reducing agent) to MB (oxidizing agent) stimulates the redox reaction, causing the dye breakdown as illustrated in Fig. 2. However, the de-colorization of MB in the occurrence of $NaBH_4$ was time-consuming. The incorporation of pristine and doped BaO in above reaction acts as an electron relay that shifts the electron from BH_4^- to MB. The shape, surface area, and crystallinity of prepared NPs influence the CA.

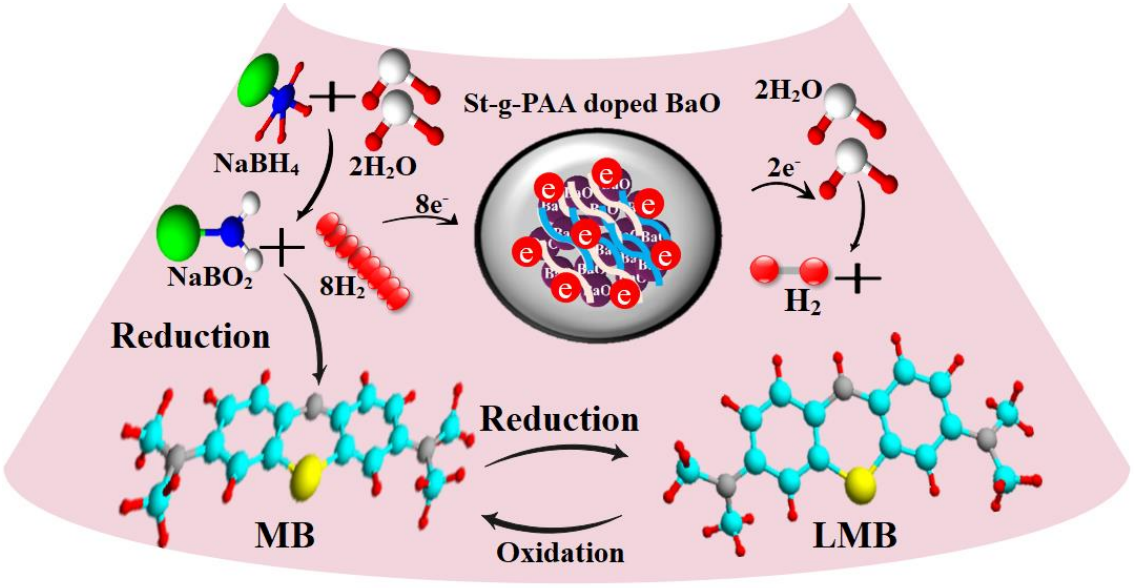

Fig. 2 Catalysis of St-g-PAA doped BaO NPs

2.6 Isolation of *S. aureus* and *E. coli*

Bovine mastitis fluids were acquired from different hospitals and cultivated at 5% blood agar and incubated for 1 day. The obtained colonies were strained on Mannitol salt agar (MSA) and

MacConkey agar (MA) to identify G ±ve microbes, respectively. Biochemical (coagulase and catalase) and gram staining techniques were utilized to isolate distinct colonies.

2.7 Antimicrobial Activity

The bactericidal efficacy of pure and doped BaO was assessed using agar well diffusion methods to test its effectiveness against isolated G +ve and G –ve microbes. After swabbing the MSA and MA deposited petri dish with isolated G +ve and G –ve cultures (1.5 x 108 CFU mL^{-1}), wells with a diameter of 6 mm were created in the MSA and MA petri dish using a sterile cork borer. Each sample was fed into wells at 500 µg/50 µL as the lowest and 1000 µg/50 µL as the highest concentration, compared to standard ciprofloxacin (5 µg/50 µL) and negative control 50 µL DI water without targeted sample. To determine whether or not NPs had an antibacterial effect, prepared plates were left in an incubator at 37 degrees Celsius for 24–48 hours. After incubation for 48 hours, an inhibition area was determined using a Vernier caliper (in millimeters), and the correlation between that area and doping levels was investigated

2.8 Molecular docking studies

Molecular docking predictions were conducted against enoyl-[acylcarrier-protein] reductase (FabI) and beta-lactamase enzyme as both these are essential for bacterial growth [27]. The 3D structural coordinates of selected enzyme targets were achieved from the protein data repository (https://www.rcsb.org/), with PDB ID as 4CUZ for $FabI_{S.\ aureus}$ [28], 4D46 for $FabI_{E.coli}$ [29], 1MWU for beta $lactamase_{S.\ aureus}$ [30], and 4KZ6 for beta $lactamase_{E.\ coli}$ [31]. ICM Molsoft was employed to conduct docking studies [32]. The protein structures were prepared using a multiple-step process, i.e., 1. Removal of H_2O molecules as well as native ligands, 2. Addition of polar H-atoms and gastegier charges, 3. Optimization of protein structure using energy minimization tool of Molsoft. Binding site was identified by specifying 10 Å area around native

ligand. Top ten docked conformation were produced in each case to get the best-docked pose of a stable complex.

Ligands structure were prepared using ligedit tool of Molsoft by modifying starch monomer structure retrieved from PubChem and stable conformation was generated for both nanocomposites in current study. 3D visualizers of Molsoft and PyMOL were used for analysis and graphical representations.

3 RESULTS AND DISCUSSION

The crystallinity of pure, dopant, and St-g-PAA incorporated BaO NPs were investigated through XRD in the 2θ range of 20°–75° (Fig. 3a). The characteristics peaks at 26.9° (101), 33.10° (110), 41° (111), 51°(201), and 60° (220) attributed to the tetragonal structure of BaO NPs along space group P4/nmm (JCPDS Card No 26-0178) [33]. Furthermore, the peak of St was observed at 25.5°. Since the PAA was incorporated into St crystalline structure, the mixtures became amorphous [34]. An additional peak was sited at 39° attributed to potassium persulphate, which was utilized in the preparation of St-g-PAA [35]. Using Scherrer's formula, the average crystallite size of the BaO and doped BaO was observed from 14.2 to 9.09 nm. The broadness of peaks was increased upon doping of St-g-PAA assigned to a decrease in the crystallinity of the NPs due to the amorphous behavior of dopant [36].

To investigate the functional group presence in BaO, dopant, and doped NPs, FTIR spectra have been utilized in range of 4000 to 500 cm^{-1}, as indicated in Fig. 3(b). The transmission band at 692 cm^{-1} represents the Ba–O bond and band at 1455 cm^{-1} might be attributed to the production of barium carbonate as a result of atmospheric CO_2 absorption by BaO [16]. The bands at 1630 and 3313 cm^{-1} indicate the H_2O symmetric vibration and O-H stretching vibration,

correspondingly. The symmetric and asymmetric COO^- stretching of acrylic acid is represented by dopant bands at 1400 and 600 cm^{-1}, respectively [37]. Additionally, SAED analysis shows bright rings related to planes (110), (222), and (202) of BaO and doped BaO (Fig. 3c-f).

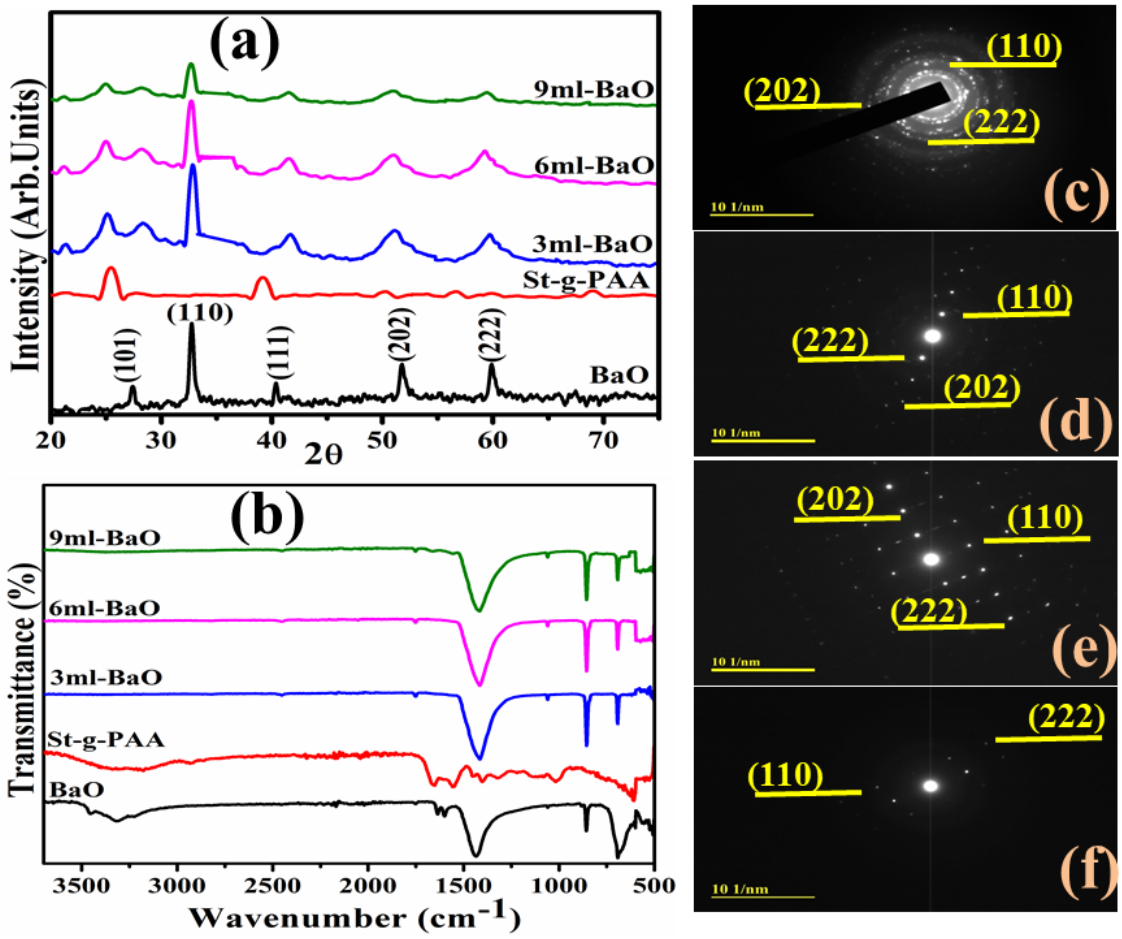

Fig. 3 (a) XRD pattern (b) FTIR spectra of BaO, dopant, and doped NPs, and (c-f) SAED patterns of pure and St-g-PAA (3,6, &9mL) doped BaO NPs respectively.

Electronic spectroscopy was employed to determine the electronic structure of synthesized NPs (Fig .4a). The light absorption of undoped BaO was seen around ~ 310 nm is attributed to the shifting of an electron from 2p of VB of O to Ba of CB correspondingly [26]. Upon doping of St-g-PAA, a red shift was observed, pointing to morphological effects with multiple active sites or possibly a quantum confinement process [38]. The direct bandgap energy of BaO, dopant,

and incorporated BaO were found to be 4.00-3.79 eV by Tauc's equation as illustrated in Fig .4(b). The low orientation rearrangement and less crystallinity of NPs may have contributed to the Eg of the St-g-PAA doped BaO decreasing as the crystallite size reduced [36].

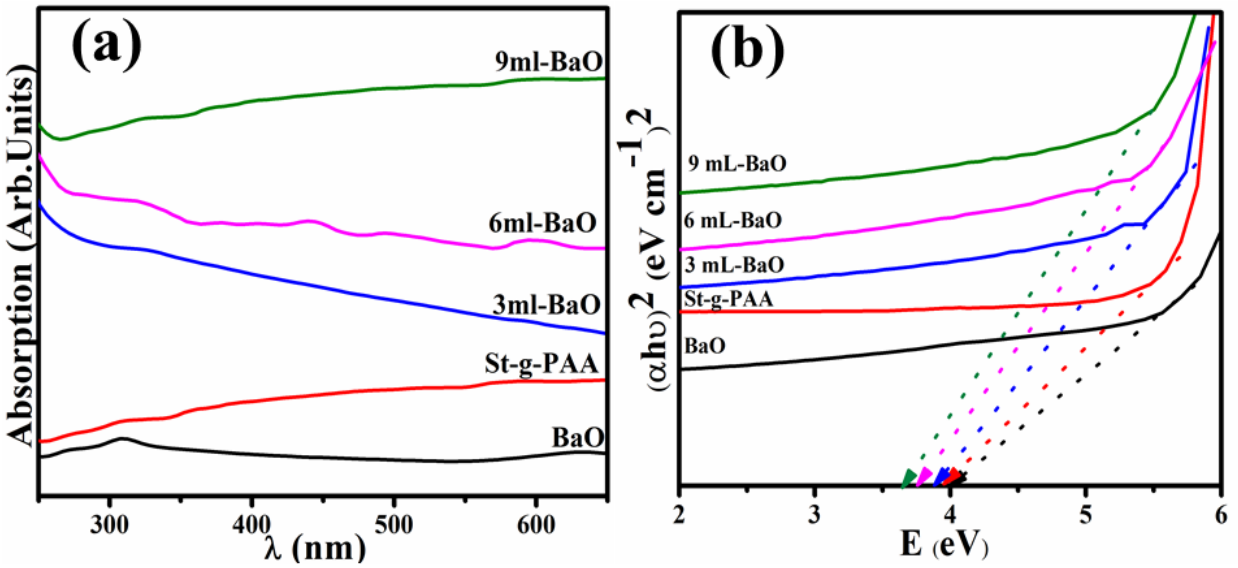

Fig. 4 (a) Electronic spectra and (b) band gap energy of BaO, St-g-PAA, and doped BaO

EDS was deployed to determine the constituent components of prepared samples, as shown in Fig 5(a-d). The existence of Ba and O peaks verified the creation of BaO. Additional peaks of Na was detected in all samples attributed to utilizing NaOH to sustain the pH during catalyst synthesis [39]. Au peak was detected due to the coating of Au sprayed over prepared materials to reduce charging influence [40]. Peak of K was seen in (Fig. 5b) as a precursor K_2SO_4 used to prepare St-g-PAA.

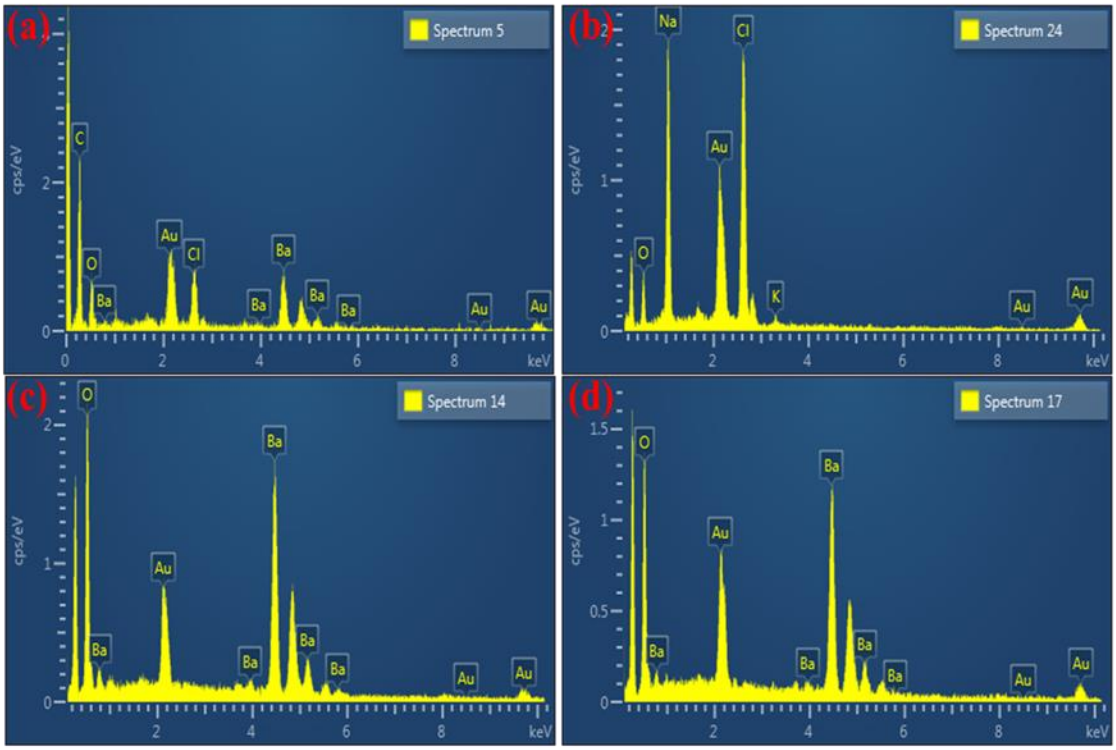

Fig. 5(a) EDS spectra of BaO (b) BaO-St-g-PAA (3,6, and 9mL) doped BaO, respectively.

Fig. 6(a-d) demonstrates the FESEM images of BaO, St-g-PAA, and doped BaO. BaO showed a chunk-like structure with unequal small-sized NPs, as shown in Fig. 6(a). Upon doping of St-g-PAA, a rod-shaped structure was observed that interacts with NPs, as demonstrated in Fig. 6(b). The diameter of nanorods was increased upon the higher concentration of St-g-PAA, as illustrated in Fig. 6(c-d).

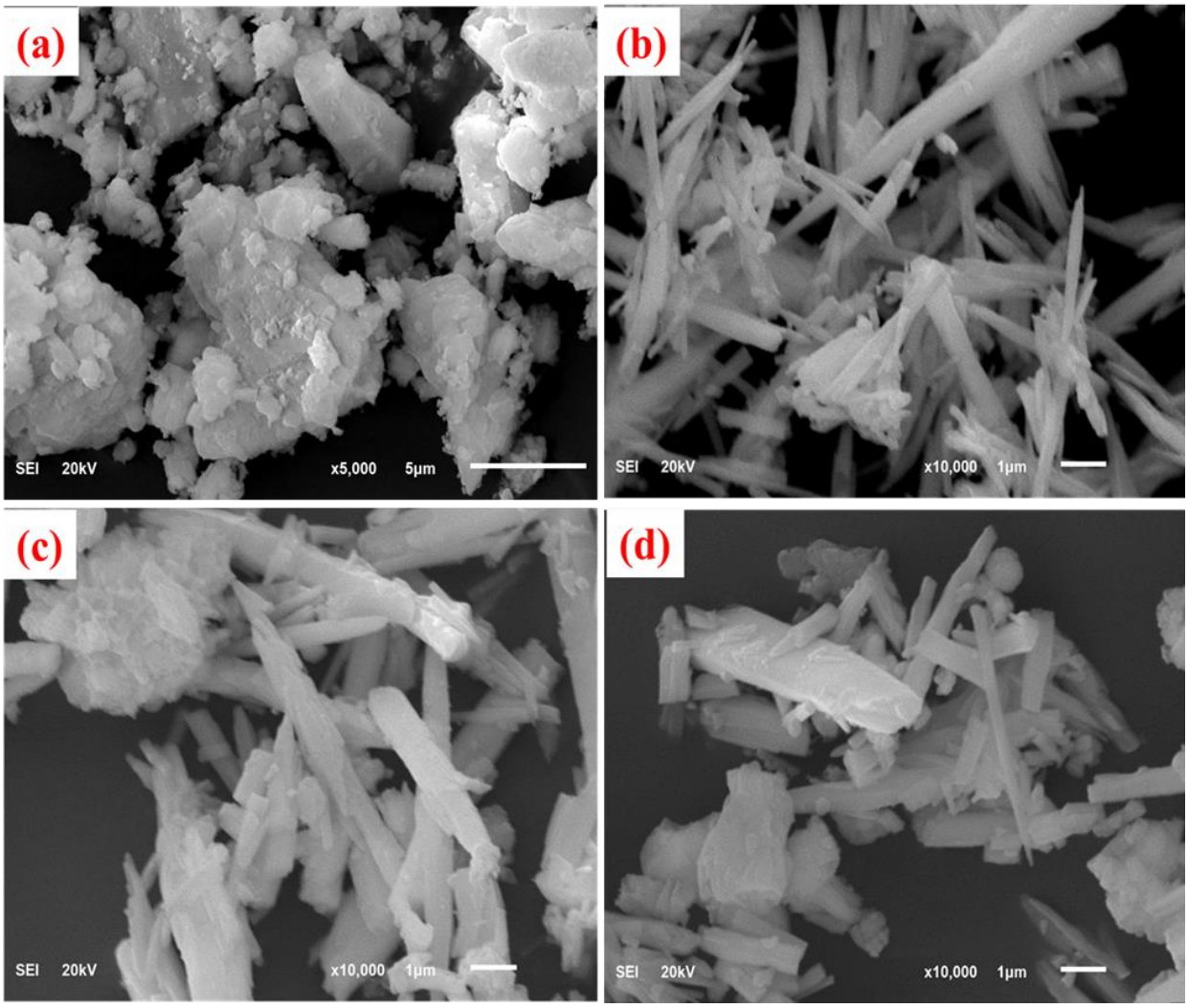

Fig. 6 (a-d) SEM analysis of BaO and St-g-PAA (3, 6, and 9 mL) doped BaO, respectively.

TEM was utilized to additional characterize the morphology and microstructure of pure and St-g-PAA-doped BaO NPs. The cubic-shaped morphology of BaO NPs is deliberated in Fig. 7(a). Fig. 7(b) demonstrates the high agglomeration of overlapped NPs. The doped samples exhibited a rod-like morphology that partially overlapped with NPs, as represented in Fig. 7(b-d). Interlayer spacing of BaO, St-g-PAA, and St-g-PAA doped BaO (3 and 6 mL) was calculated from a plane (101) as 0.17, 0.29, 0.32 and 0.22 nm, correspondingly that is well matched with XRD data as shown in Fig. 7(á-d´).

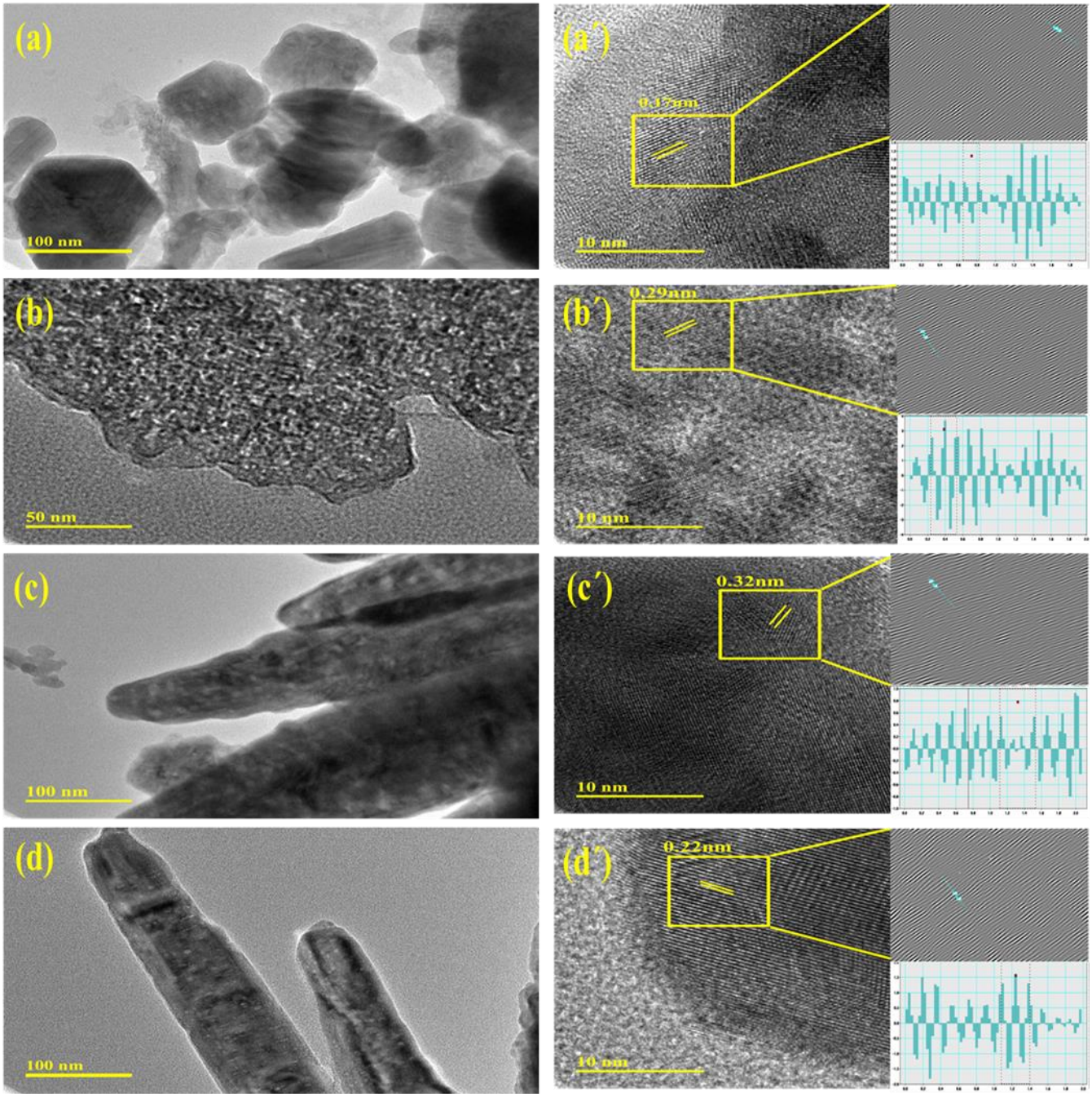

Fig. 7 (a-d) HR-TEM micrographs and, (á-d´) d-spacing of pure, St-g-PAA, and St-g-PAA (3 and 6 mL) doped BaO.

CA of pure, grafted, and doped BaO NPs in the occurrence of $NaBH_4$ for MB reduction was examined through a UV-Vis spectrophotometer. All samples explored maximum reduction of MB 61.6-75.1% in a neutral environment (pH~7), 67.8-79.9% in an acidic environment

(pH~3.5), and 61.7-97.6% in basic condition (pH~11.5) as demonstrated in Fig. 8(a-c), correspondingly. The crystal structure, particle size, and shape of the synthesized catalyst influenced the CA. Synthesized materials in the existence of $NaBH_4$ function as electron relays which shift the electron from BH_4^- to dye, causing the de-colorization of MB. NPs showed significant active sites that elevate the adsorption of MB and BH_4^-, which promotes the dye reduction efficacy. In an acidic environment, maximum reduction for 9 mL doped BaO attributed to a larger production of H^+ ion on catalyst surface. CA in a basic environment showed good results because of higher electrostatic interaction among negatively charged catalyst and positively charged MB dye. In a basic medium, catalysts get a negative charge on their surface, while the reduction of cationic MB in an acidic environment is hindered by positively charged catalyst surface [41] [42].

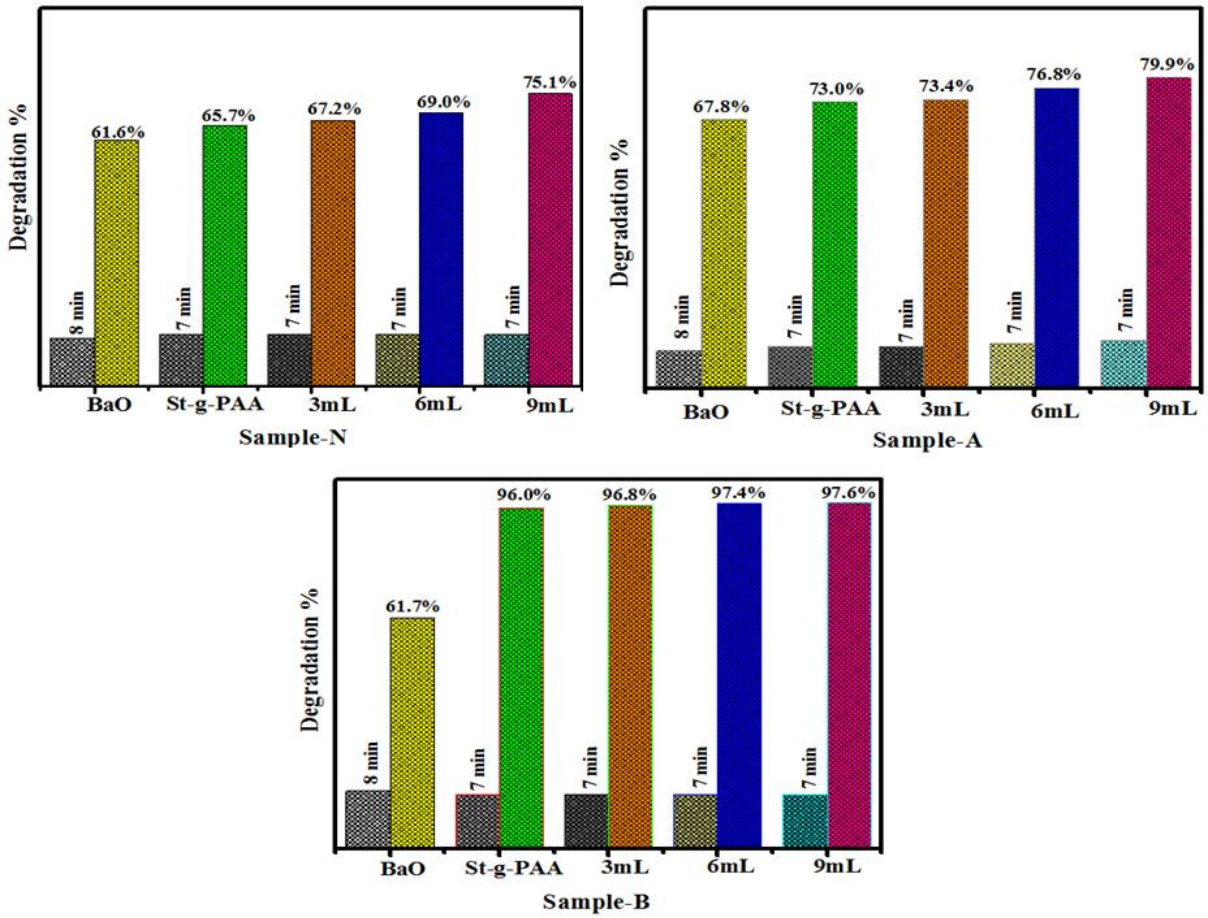

Fig. 8 Catalysis of BaO and St-g-PAA doped BaO (a) in neutral (b) Acidic and (c) Basic

3.1 Antimicrobial Activity

Antimicrobial performance of pure, St-g-PAA, and incorporated BaO were conducted by utilizing a well diffusion approach contrary to *S.aureus* and *E.coli* as represented in Table 1. At high concentrations, substantial inhibition zones ($P < 0.05$) for G ±ve were confirmed as (1.55 – 2.40 mm) for *E. coli* and (3.15-7.35 mm) for *S. aureus*, respectively. In contrast to DI water (0 mm), ciprofloxacin had an inhibition zone of 4.25 and 9.20 mm beside *E. coli* and *S. aureus*, correspondingly. In contrast to *E.coli*, synthesized NPs exhibited an increased antibacterial efficacy against *S. aureus* because cell wall of G -ve is thicker consisting large complex structure

than G +ve bacteria. The antibacterial efficacy of NPs assigned to different factors, including electrostatic relations of OH and H_2O_2 on the surface, which produce the reactive oxygen species (ROS) as demonstrated in Fig. 9. This caused the oxidative stress on bacteria's cell walls, resulting in the death of cells [43]. According to experimental findings, St-g- PAA dopant enhances BaO's antibacterial activity against *S. aureus* bacteria [18].

Table 1 Antimicrobial activity of St-g-PAA doped BaO

Samples	[1]Inhibition zone (mm)		[2]Inhibition zone (mm)	
	0.5mg/50µL	1.0mg/50µL	0.5mg/50µL	1.0mg/50µL
BaO	0	0	0	0
St-g-PAA	0	0	0	0
(3 mL)St-g-PAA: BaO	0	3.15	0	0
(6 mL)St-g-PAA:BaO	0	6.05	0	1.55
(9 mL)St-g-PAA:BaO	0	7.35	0	2.40
Ciprofloxacin	9.20	9.20	4.25	4.25
DIW	0	0	0	0

[1] Inhibition zones for *S.aureus*

[2] Inhibition zones for *E.coli*

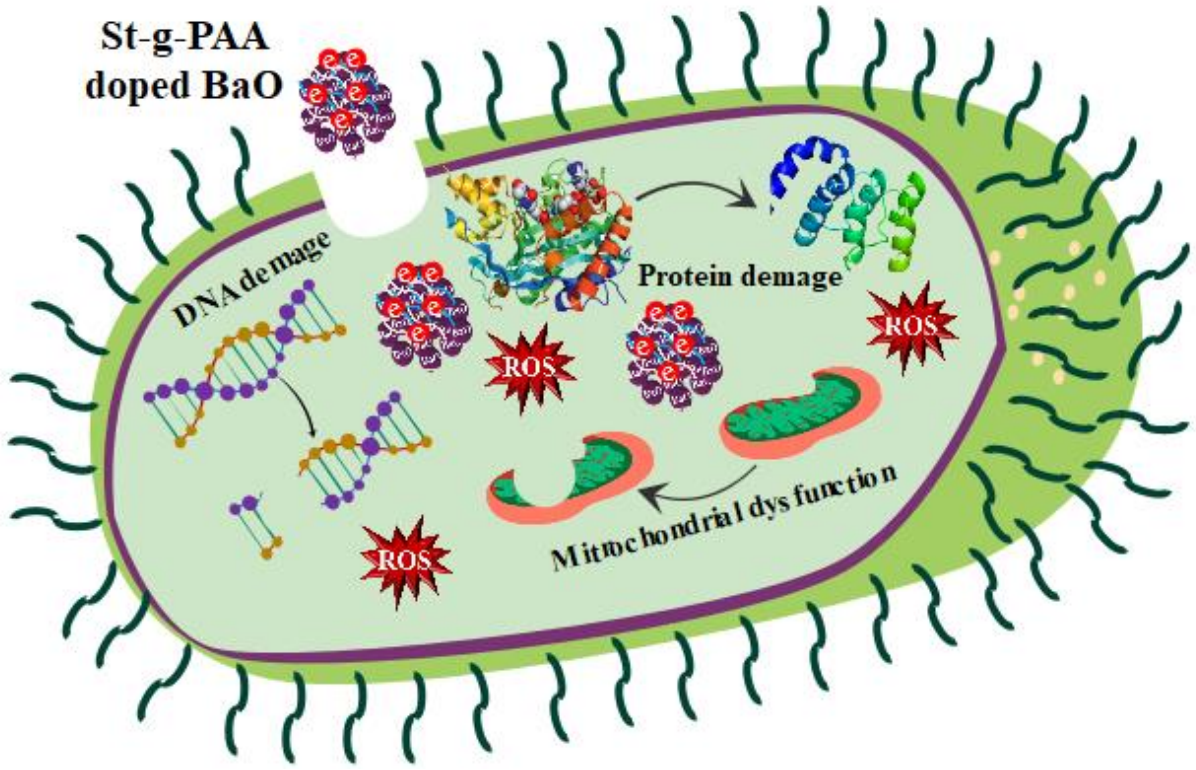

Fig. 9 Antibacterial mechanism of St-g-PAA doped BaO.

3.2 Molecular docking studies:

The role of nanoparticles as potential bactericidal agents have been extensively reported still the mystery behind this potency needs to be explored. Disruption of various cell processes by inhibiting enzyme targets has been considered an effective strategy for exploring new antibacterial agents [6,10]. Computational techniques represent a valuable source to predict possible mechanisms governing these biological activities, particularly molecular docking predictions [44,45]. In the case of FabI$_{S.\ aureus}$, both st-g-PAA and St-g-PAA doped BaO nanocomposites revealed good binding scores of -7.923 kcal/mol and -6.057 kcal/mol, respectively. Four H-bonds, i.e., Gly13 (2.7Å), Arg40 (2.6 Å), Ala95 (2.8 Å), Ser197 (2.7 Å), and two hydrophobic interactions with Ala15 and Ile94 served as main contributor towards the docked complex formation of st-g-PAA nanocomposite (Fig. 10A). Similarly, St-g-PAA doped

BaO nanocomposite complex with FabI$_{S.\ aureus}$ showed involvement of multiple H-bonds like Gly191 (3.1 Å), Thr195 (1.9 Å), and Ser197 (2.6 Å) alongside hydrophobic interactions with Ile20 and Thr145 as depicted in Fig. 10 B. On the contrary, docked complexes formed inside the active pocket of FabI$_{E.coli}$ showed differences in binding approach of st-g-PAA and St-g-PAA doped BaO nanocomposites. A docked complex formed in case of St-g-PAA doped BaO nanocomposites showed involvement of hydrophobic interactions as main factor for binding along with two H-bonds, i.e., Ser91 (3.0 Å) and Tyr156 (2.7 Å) having binding score -5.919 kcal/mol. On the other hand, st-g-PAA nanocomposite docked complex revealed multiple H-bonds like Ala21 (3.4 Å), Gly13 (3.0 Å), Ser19 (2.6 Å) and Lys163 (2.7 Å) along with hydrophobic interaction to Ile20 as shown in Figure 10 C & D.

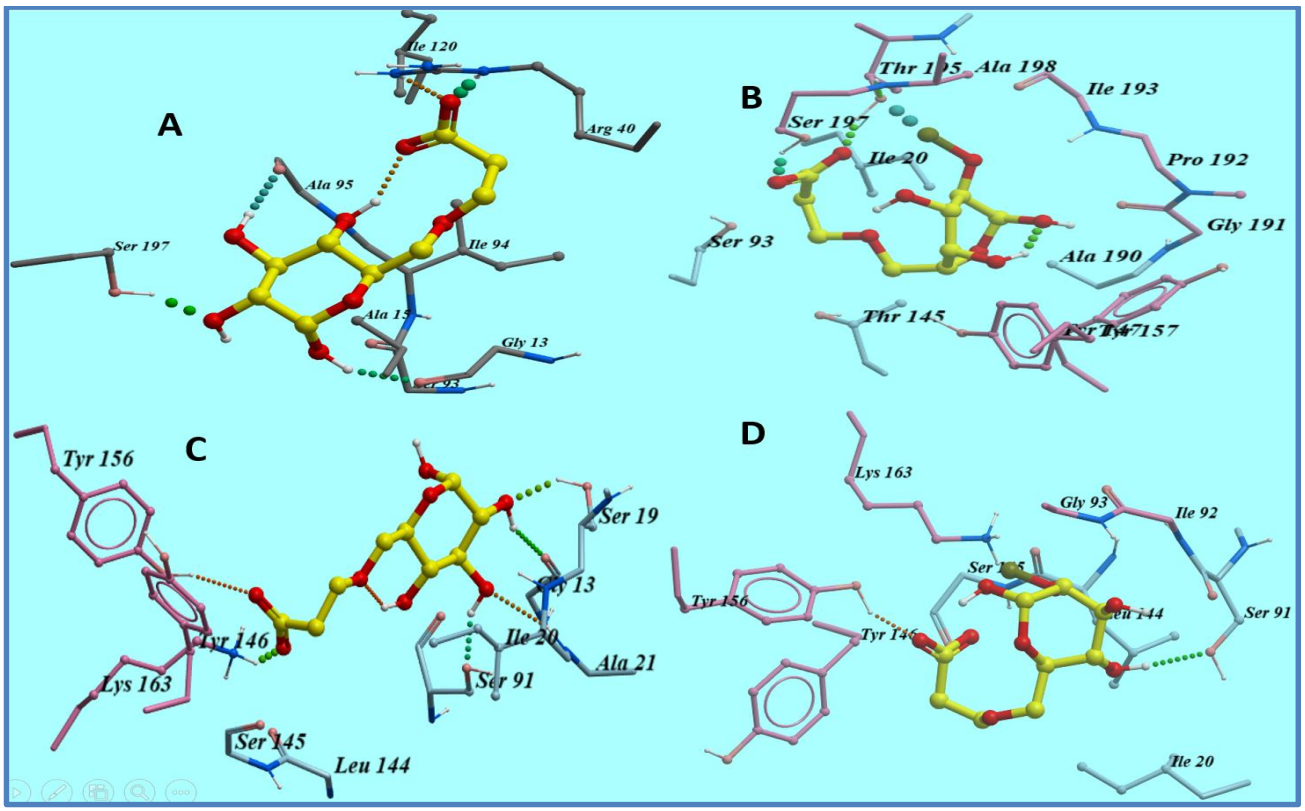

Fig. 10 Graphical representation of binding site interactions of FabI for St-g-PAA and St-g-PAA doped BaO nanocomposite A & B from *S. aureus* and C & D from *E. coli*

The second enzyme target selected was beta-lactamase, which is essential for bacterial survival and previously reported as an important target for discovering new antibiotics. Both these nanocomposites St-g-PAA and St-g-PAA doped BaO were evaluated for their binding mode and docked complex formation tendency within active site of beta lactamase$_{S.\ aureus}$. St-g-PAA showed three H-bond interactions with Ser403 (3.0 Å), Thr600 (2.9 Å), and Lys597 (3.3 Å), while Tyr446 and Ser462 were involved in hydrophobic interactions with a binding score as -5.598 kcal/mol. Similarly, four H-bonds were observed for St-g-PAA doped BaO nanocomposite docked complex as Asn464 (3.3 Å), His583 (2.6 Å), Ser598 (2.8 Å) and Thr600 (2.8 Å) along with pi-pi interaction with Tyr446 and other hydrophobic interactions (Fig. 11A & B). The binding score observed for St-g-PAA doped BaO nanocomposite-beta lactamase$_{S.\ aureus}$ docked complex was -9.101 kcal/mol.

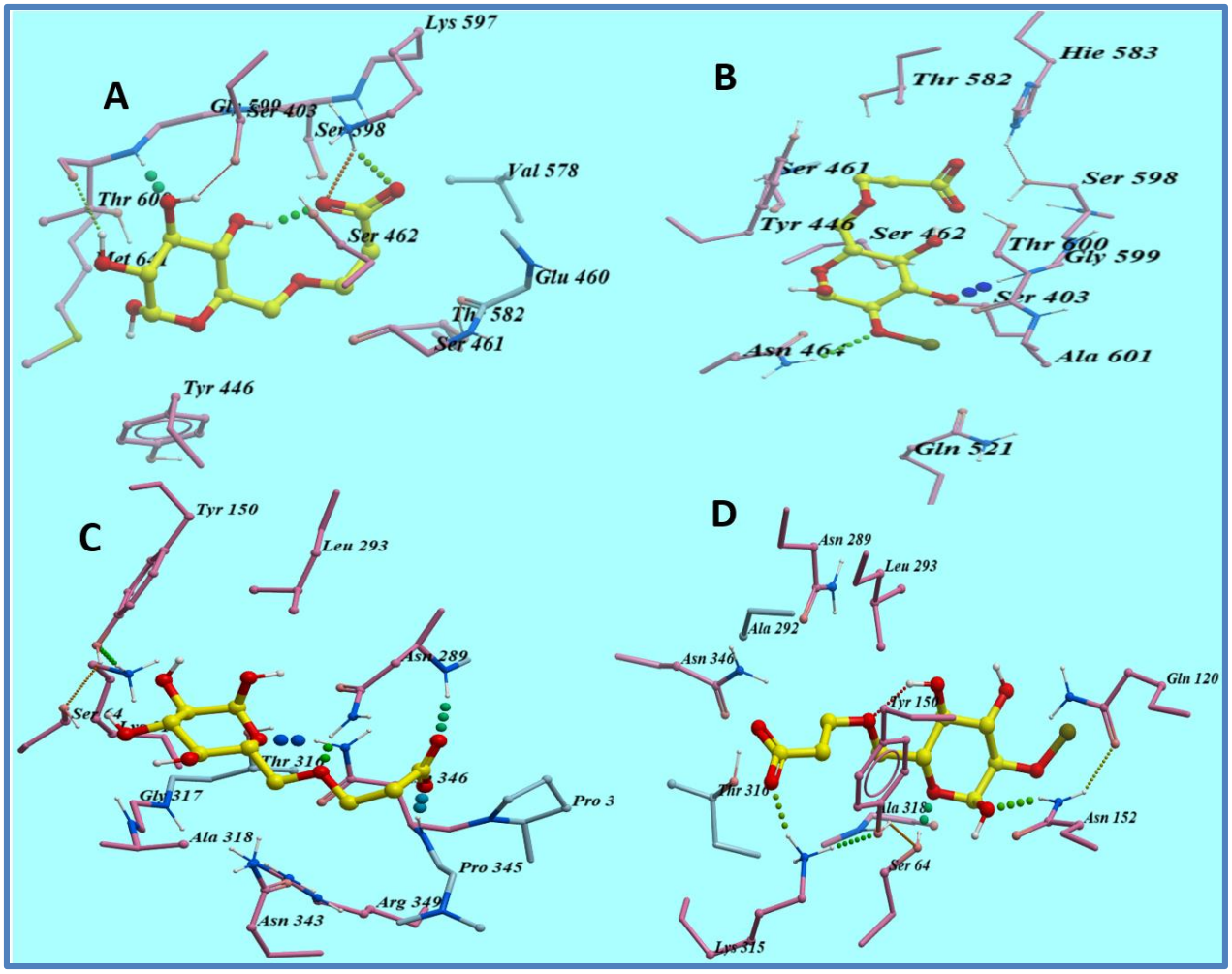

Fig. 11 Graphical representation of binding site interactions of beta-lactamase for St-g-PAA and St-g-PAA doped BaO nanocomposite A & B from *S. aureus* and C & D from *E. coli*

Also, in the case of St-g-PAA docked complex with beta lactamase$_{E.\ coli}$, Tyr150 revealed pi-pi interaction while Asn289 and Asn346 formed H-bonds having distances of 2.2 Å and 2.5 Å, respectively, with a score of -6.696 kcal/mol. St-g-PAA doped BaO nanocomposite showed similar binding patterns like the involvement of pi-pi correlation with Tyr150 and three H-bonds as Ser64 (2.5 Å), Asn152 (2.9 Å), Lys315 (2.7 Å) along with hydrophobic relation with Lys293 having docking score -7.783 kcal/mol (Fig 11C & D).

4 CONCLUSION

In order to determine the antibacterial and catalytic activity, different concentrations of St-g-PAA doped BaO NPs were effectively produced by a simple co-precipitation method. BaO has tetragonal structure confirmed by the XRD pattern, which showed that reduction in crystallinity upon dopants. FTIR was used to confirm the occurrence of functional groups in prepared NPs and polycrystalline nature of BaO was validated through SAED. According to UV-Vis spectra, doping caused to decrease the bandgap energy from 4.00 to 3.79 eV. The d-spacing (0.17, 0.29, 0.32, and 0.22 nm) was calculated using HR-TEM, which correlates with XRD. The maximum catalytic degradation of MB was observed at 97% for doped samples in a basic environment. Additionally, the bactericidal efficacy of the BaO NPs was determined against the bacteria *S. aureus* and *E. coli* (0-2.40 mm)*;* while higher antibacterial performance was observed by the *S. aureus* (0-7.35 mm) at higher concentration compared to and *E. coli* (0-2.40 mm) upon doping. In silico studies were carried out against enoyl-[acylcarrier-protein] reductase (FabI) and beta-lactamase enzyme to assess St-g-PAA and St-g-PAA doped BaO nanocomposites as inhibitors and elucidates their mode of action. From these results, we conclude that St-g-PAA doped BaO NPs can be used as ideal catalyst in basic media and potential inhibitor.

Acknowledgment: Thanks to higher education commission (HEC), Pakistan for NRPU-20-17615 (Muhammad Ikram).

REFERENCES

[1] M.M. Hasan, M.A. Shenashen, M.N. Hasan, H. Znad, M.S. Salman, M.R. Awual, Natural biodegradable polymeric bioadsorbents for efficient cationic dye encapsulation from wastewater, J. Mol. Liq. 323 (2021). https://doi.org/10.1016/j.molliq.2020.114587.

[2] S. Moniri Javadhesari, S. Alipour, S. Mohammadnejad, M.R. Akbarpour, Antibacterial activity of ultra-small copper oxide (II) nanoparticles synthesized by mechanochemical processing against S. aureus and E. coli, Mater. Sci. Eng. C. 105 (2019). https://doi.org/10.1016/j.msec.2019.110011.

[3] R.N. Bharagava, G. Saxena, S.I. Mulla, Introduction to Industrial Wastes Containing Organic and Inorganic Pollutants and Bioremediation Approaches for Environmental Management, in: Bioremediation Ind. Waste Environ. Saf., Springer Singapore, 2020: pp. 1–18. https://doi.org/10.1007/978-981-13-1891-7_1.

[4] A. Raza, M. Ikram, M. Aqeel, M. Imran, A. Ul-Hamid, K.N. Riaz, S. Ali, Enhanced industrial dye degradation using Co doped in chemically exfoliated MoS2 nanosheets, Appl. Nanosci. 10 (2020) 1535–1544. https://doi.org/10.1007/s13204-019-01239-3.

[5] M.M. Ghangrekar, P. Chatterjee, Water pollutants classification and its effects on environment, in: Carbon Nanostructures, Springer International Publishing, 2018: pp. 11–26. https://doi.org/10.1007/978-3-319-95603-9_2.

[6] M. Ikram, A. Mahmood, A. Haider, S. Naz, A. Ul-Hamid, W. Nabgan, I. Shahzadi, J. Haider, I. Ahmad, S. Ali, Dye degradation, antibacterial and in-silico analysis of Mg/cellulose-doped ZnO nanoparticles, Int. J. Biol. Macromol. 185 (2021) 153–164. https://doi.org/10.1016/j.ijbiomac.2021.06.101.

[7] B.C. Hodges, E.L. Cates, J.H. Kim, Challenges and prospects of advanced oxidation water treatment processes using catalytic nanomaterials, Nat. Nanotechnol. 13 (2018) 642–650. https://doi.org/10.1038/s41565-018-0216-x.

[8] M. Rafatullah, O. Sulaiman, R. Hashim, A. Ahmad, Adsorption of methylene blue on low-cost adsorbents: A review, J. Hazard. Mater. 177 (2010) 70–80. https://doi.org/10.1016/j.jhazmat.2009.12.047.

[9] M.D.A. Khan, A. Akhtar, S.A. Nabi, M.A. Khan, Synthesis, characterization, and photocatalytic activity of polyaniline-Sn(IV)iodophosphate nanocomposite: Its application in wastewater detoxification, Ind. Eng. Chem. Res. 53 (2014) 15253–15260. https://doi.org/10.1021/ie502804s.

[10] A. Rafiq, M. Ikram, S. Ali, F. Niaz, M. Khan, Q. Khan, M. Maqbool, Photocatalytic degradation of dyes using semiconductor photocatalysts to clean industrial water pollution, J. Ind. Eng. Chem. 97 (2021) 111–128. https://doi.org/10.1016/j.jiec.2021.02.017.

[11] M. Serhan, M. Sprowls, D. Jackemeyer, M. Long, I.D. Perez, W. Maret, N. Tao, E. Forzani, Total iron measurement in human serum with a smartphone, in: AIChE Annu. Meet. Conf. Proc., 2019: pp. 1–3. https://doi.org/10.1039/x0xx00000x.

[12] A. Arshad, J. Iqbal, M. Siddiq, M.U. Ali, A. Ali, H. Shabbir, U. Bin Nazeer, M.S. Saleem, Solar light triggered catalytic performance of graphene-CuO nanocomposite for waste water treatment, Ceram. Int. 43 (2017) 10654–10660. https://doi.org/10.1016/j.ceramint.2017.03.165.

[13] H. Wang, J.Z. Xu, J.J. Zhu, H.Y. Chen, Preparation of CuO nanoparticles by microwave irradiation, J. Cryst. Growth. 244 (2002) 88–94. https://doi.org/10.1016/S0022-0248(02)01571-3.

[14] F. Naz, K. Saeed, Synthesis of barium oxide nanoparticles and its novel application as a catalyst for the photodegradation of malachite green dye, Appl. Water Sci. 12 (2022). https://doi.org/10.1007/s13201-022-01649-9.

[15] R. Gillani, B. Ercan, A. Qiao, T.J. Webster, Nanofunctionalized zirconia and barium sulfate particles as bone cement additives, Int. J. Nanomedicine. 5 (2010) 1–11. https://doi.org/10.2147/ijn.s7603.

[16] M.S. Mauter, I. Zucker, F. Perreault, J.R. Werber, J.H. Kim, M. Elimelech, The role of nanotechnology in tackling global water challenges, Nat. Sustain. 1 (2018) 166–175. https://doi.org/10.1038/s41893-018-0046-8.

[17] A. Biswal, P.K. Sethy, S.K. Swain, Change in Orientation of Polyacrylic Acid and Chitosan Networks by Imprintment of Gold Nanoparticles, Polym. Technol. Mater. 60 (2021) 182–194. https://doi.org/10.1080/25740881.2020.1793196.

[18] F. Jamal, M. Ikram, A. Haider, A. Ul-Hamid, M. Ijaz, W. Nabgan, J. Haider, I. Shahzadi, Facile synthesis of silver and polyacrylic acid doped magnesium oxide nanostructure for photocatalytic dye degradation and bactericidal behavior, Appl. Nanosci. 12 (2022) 2409–2419. https://doi.org/10.1007/s13204-022-02504-8.

[19] Y. Tang, Y. Li, Y. Zhang, C. Mu, J. Zhou, W. Zhang, B. Shi, Nonswelling Silica-Poly(acrylic acid) Composite for Efficient and Simultaneous Removal of Cationic Dye, Heavy Metal, and Surfactant-Stabilized Emulsion from Wastewater, Ind. Eng. Chem. Res. 59 (2020) 3383–3393. https://doi.org/10.1021/acs.iecr.9b05120.

[20] A. Saberi, E. Alipour, M. Sadeghi, Superabsorbent magnetic Fe3O4-based starch-poly

(acrylic acid) nanocomposite hydrogel for efficient removal of dyes and heavy metal ions from water, J. Polym. Res. 26 (2019). https://doi.org/10.1007/s10965-019-1917-z.

[21] M.R. Shaik, M. Kuniyil, M. Khan, N. Ahmad, A. Al-Warthan, M.R.H. Siddiqui, S.F. Adil, D.J. McPhee, Modified polyacrylic acid-zinc composites: Synthesis, characterization and biological activity, Molecules. 21 (2016). https://doi.org/10.3390/molecules21030292.

[22] L. Boels, G.J. Witkamp, Carboxymethyl inulin biopolymers: A green alternative for phosphonate calcium carbonate growth inhibitors, Cryst. Growth Des. 11 (2011) 4155–4165. https://doi.org/10.1021/cg2007183.

[23] M. Ikram, S. Hayat, M. Imran, A. Haider, S. Naz, A. Ul-Hamid, I. Shahzadi, J. Haider, A. Shahzadi, W. Nabgan, S. Ali, Novel Ag/cellulose-doped CeO2 quantum dots for efficient dye degradation and bactericidal activity with molecular docking study, Carbohydr. Polym. 269 (2021). https://doi.org/10.1016/j.carbpol.2021.118346.

[24] S. Shaheen, A. Iqbal, M. Ikram, K. Ul-Ain, S. Naz, A. Ul-Hamid, A. Shahzadi, A. Haider, W. Nabgan, J. Haider, Effective Disposal of Methylene Blue and Bactericidal Benefits of Using GO-Doped MnO2Nanorods Synthesized through One-Pot Synthesis, ACS Omega. 6 (2021) 24866–24878. https://doi.org/10.1021/acsomega.1c03723.

[25] N. Bahadoran Baghbadorani, T. Behzad, M.H. Karimi Darvanjooghi, N. Etesami, Modelling of water absorption kinetics and biocompatibility study of synthesized cellulose nanofiber-assisted starch-graft-poly(acrylic acid) hydrogel nanocomposites, Cellulose. 27 (2020) 9927–9945. https://doi.org/10.1007/s10570-020-03511-0.

[26] M.A. Ansari, N. Jahan, Structural and Optical Properties of BaO Nanoparticles

Synthesized by Facile Co-precipitation Method, Mater. Highlights. 2 (2021) 23. https://doi.org/10.2991/mathi.k.210226.001.

[27] S.M. Drawz, R.A. Bonomo, Three decades of β-lactamase inhibitors, Clin. Microbiol. Rev. 23 (2010) 160–201. https://doi.org/10.1128/CMR.00037-09.

[28] J. Schiebel, A. Chang, S. Shah, Y. Lu, L. Liu, P. Pan, M.W. Hirschbeck, M. Tareilus, S. Eltschkner, W. Yu, J.E. Cummings, S.E. Knudson, G.R. Bommineni, S.G. Walker, R.A. Slayden, C.A. Sotriffer, P.J. Tonge, C. Kisker, Rational design of broad spectrum antibacterial activity based on a clinically relevant enoyl-acyl carrier protein (ACP) reductase inhibitor, J. Biol. Chem. 289 (2014) 15987–16005. https://doi.org/10.1074/jbc.M113.532804.

[29] J. Schiebel, A. Chang, B. Merget, G.R. Bommineni, W. Yu, L.A. Spagnuolo, M. V Baxter, M. Tareilus, P.J. Tonge, C. Kisker, C.A. Sotriffer, An Ordered Water Channel in Staphylococcus aureus FabI: Unraveling the Mechanism of Substrate Recognition and Reduction, Biochemistry. 54 (2015) 1943–1955. https://doi.org/10.1021/bi5014358.

[30] D. Lim, N.C.J. Strynadka, Structural basis for the β-lactam resistance of PBP2a from methicillin-resistant Staphylococcus aureus, Nat. Struct. Biol. 9 (2002) 870–876. https://doi.org/10.1038/nsb858.

[31] S. Barelier, O. Eidam, I. Fish, J. Hollander, F. Figaroa, R. Nachane, J.J. Irwin, B.K. Shoichet, G. Siegal, Increasing chemical space coverage by combining empirical and computational fragment screens, ACS Chem. Biol. 9 (2014) 1528–1535. https://doi.org/10.1021/cb5001636.

[32] R. Abagyan, M. Totrov, Biased probability Monte Carlo conformational searches and electrostatic calculations for peptides and proteins, J. Mol. Biol. 235 (1994) 983–1002. https://doi.org/10.1006/jmbi.1994.1052.

[33] A.Z. Bazeera, M.I. Amrin, Synthesis and Characterization of Barium Oxide Nanoparticles, IOSR J. Appl. Phys. 01 (2017) 76–80. https://doi.org/10.9790/4861-17002017680.

[34] O.A. Bin-Dahman, J. Jose, M.A. Al-Harthi, Compatibility of poly(acrylic acid)/starch blends, Starch/Staerke. 67 (2015) 1061–1069. https://doi.org/10.1002/star.201500011.

[35] N. C, Y. K V, M.P. R, S. M, G.B. R, Simultaneous refining of biodiesel-derived crude glycerol and synthesis of value-added powdered catalysts for biodiesel production: A green chemistry approach for sustainable biodiesel industries, J. Clean. Prod. 363 (2022). https://doi.org/10.1016/j.jclepro.2022.132448.

[36] M. Ikram, N. Abid, A. Haider, A. Ul-Hamid, J. Haider, A. Shahzadi, W. Nabgan, S. Goumri-Said, A.R. Butt, M. Benali Kanoun, Toward efficient dye degradation and the bactericidal behavior of Mo-doped La2O3nanostructures, Nanoscale Adv. 4 (2022) 926–942. https://doi.org/10.1039/d1na00802a.

[37] A. Ashfaq, M. Ikram, A. Haider, A. Ul-Hamid, I. Shahzadi, J. Haider, Nitrogen and Carbon Nitride-Doped TiO2 for Multiple Catalysis and Its Antimicrobial Activity, Nanoscale Res. Lett. 16 (2021). https://doi.org/10.1186/s11671-021-03573-4.

[38] S. K K, A. Saji, A. Chanda, M. Vasundhara, Effects of Calcinations Temperatures on Structural, optical and magnetic properties of MgO nanoflakes and its photocatalytic

applications, Opt. Mater. (Amst). 132 (2022). https://doi.org/10.1016/j.optmat.2022.112777.

[39] M. Ikram, T. Inayat, A. Haider, A. Ul-Hamid, J. Haider, W. Nabgan, A. Saeed, A. Shahbaz, S. Hayat, K. Ul-Ain, A.R. Butt, Graphene Oxide-Doped MgO Nanostructures for Highly Efficient Dye Degradation and Bactericidal Action, Nanoscale Res. Lett. 16 (2021). https://doi.org/10.1186/s11671-021-03516-z.

[40] M. Ikram, S. Aslam, A. Haider, S. Naz, A. Ul-Hamid, A. Shahzadi, M. Ikram, J. Haider, S.O.A. Ahmad, A.R. Butt, Doping of Mg on ZnO Nanorods Demonstrated Improved Photocatalytic Degradation and Antimicrobial Potential with Molecular Docking Analysis, Nanoscale Res. Lett. 16 (2021). https://doi.org/10.1186/s11671-021-03537-8.

[41] L. Yang, X. Yang, R. Zhou, Probing BaO Doping Effect on the Structure and Catalytic Performance of Pd/CexZr1-xO2 (x = 0.2-0.8) Catalysts for Automobile Emission Control, J. Phys. Chem. C. 120 (2016) 2712–2723. https://doi.org/10.1021/ACS.JPCC.5B10301.

[42] A. Bari, M. Ikram, A. Haider, A. Ul-Hamid, J. Haider, I. Shahzadi, G. Nazir, A. Shahzadi, M. Imran, A. Ghaffar, Evaluation of bactericidal potential and catalytic dye degradation of multiple morphology based chitosan/polyvinylpyrrolidone-doped bismuth oxide nanostructures, Nanoscale Adv. 4 (2022) 2713–2728. https://doi.org/10.1039/d2na00105e.

[43] M. Ikram, A. Shahzadi, S. Hayat, W. Nabgan, A. Ul-Hamid, A. Haider, M. Noor, S. Goumri-Said, M.B. Kanoun, S. Ali, Novel Ta/chitosan-doped CuO nanorods for catalytic purification of industrial wastewater and antimicrobial applications, RSC Adv. 12 (2022) 16991–17004. https://doi.org/10.1039/d2ra03006c.

[44] D. Seeliger, B.L. De Groot, Ligand docking and binding site analysis with PyMOL and Autodock/Vina, J. Comput. Aided. Mol. Des. 24 (2010) 417–422. https://doi.org/10.1007/s10822-010-9352-6.

[45] M.N. Mohamad Rosdi, S. Mohd Arif, M.H. Abu Bakar, S.A. Razali, R. Mohamed Zulkifli, H. Ya'akob, Molecular docking studies of bioactive compounds from Annona muricata Linn as potential inhibitors for Bcl-2, Bcl-w and Mcl-1 antiapoptotic proteins, Apoptosis. 23 (2018) 27–40. https://doi.org/10.1007/s10495-017-1434-7.

ABSTRACT

The removal of cationic dyes from water has received a great attention of researchers considering their influence on environment and ecosystem. In current work, starch-grafted-poly acrylic acid (St-g-PAA) doped BaO nanoparticles have been synthesized by co-precipitation approach. The aim of this research was to reduce the harmful methylene blue dye and evaluate the antibacterial activity of St-g-PAA doped BaO. XRD spectra exhibited the tetragonal structure of BaO and no variations occurred upon doping. The optical properties of St-g-PAA doped BaO have been evaluated by UV–Vis spectrophotometer. The existence of a dopant in the product was verified using EDS spectroscopy. TEM revealed the formation of cubic-shaped NPs of BaO and upon the addition of St-g-PAA, a few nanorod-like structures. The higher concentration of St-g-PAA doped BaO exhibit a remarkable reduction of methylene blue in a basic environment. Furthermore, St-g-PAA doped BaO revealed higher antimicrobial efficacy against *Staphylococcus aureus* in comparison to *Escherichia coli*. *In silico* studies were conducted against enoyl-[acylcarrier-protein] reductase (FabI) and beta-lactamase enzyme to evaluate the potential of both St-g-PAA and St-g-PAA doped BaO nanocomposites as their inhibitors and to rationalize their possible mode of action.